The EMBO Journal Vol. 20 No. 15 pp. 4107–4121, 2001

Propagation of the apoptotic signal by mitochondrial waves

Pál Pacher and György Hajnóczky[1]

Department of Pathology, Anatomy and Cell Biology, Thomas Jefferson University, Philadelphia, 1020 Locust str Suite 253 JAH, PA 19107, USA

[1]Corresponding author
e-mail: Gyorgy.Hajnoczky@mail.tju.edu

Generation of mitochondrial signals is believed to be important in the commitment to apoptosis, but the mechanisms coordinating the output of individual mitochondria remain elusive. We show that in cardiac myotubes exposed to apoptotic agents, Ca^{2+} spikes initiate depolarization of mitochondria in discrete subcellular regions, and these mitochondria initiate slow waves of depolarization and Ca^{2+} release propagating through the cell. Traveling mitochondrial waves are prevented by Bcl-x_L, involve permeability transition pore (PTP) opening, and yield cytochrome *c* release, caspase activation and nuclear apoptosis. Mitochondrial Ca^{2+} uptake is critical for wave propagation, and mitochondria at the origin of waves take up Ca^{2+} particularly effectively, providing a mechanism that may underlie selection of the initiation sites. Thus, apoptotic agents transform the mitochondria into an excitable state by sensitizing PTP to Ca^{2+}. Expansion of the local excitation by mitochondrial waves propagating through the whole cell can be especially important in activation of the apoptotic machinery in large cells.

Keywords: apoptosis/calcium/mitochondria/waves

Introduction

Cellular signals originating from discrete cellular domains often give rise to traveling messenger waves that relay the signal at full strength to remote intracellular targets or even to other cells. Recent studies have demonstrated that expansion of the local excitation is critical for the actions of second messengers (cAMP, Ca^{2+}) and have determined some fundamental properties of messenger diffusion and amplification that are utilized in the mechanisms underlying propagation of waves (reviewed in Meyer, 1991; Clapham and Sneyd, 1995; Thomas *et al*., 1996; Berridge, 1997; Berridge *et al*., 1998; Lechleiter *et al*., 1998). Evidence is emerging that mitochondria are involved in intracellular waves in a number of ways. Our studies have demonstrated that mitochondrial redox waves are coupled to inositol 1,4,5-trisphosphate (IP_3) receptor (IP_3R)-driven cytosolic [Ca^{2+}] ($[Ca^{2+}]_c$) waves (Hajnóczky *et al*., 1995). Mitochondrial redox waves have also been shown to result from intrinsic oscillations of metabolism (Romashko *et al*., 1998). These waves have been thought to be important in the control of mitochondrial ATP formation. During IP_3R-driven Ca^{2+} spiking, mitochondrial Ca^{2+} uptake has also been demonstrated to modulate the propagation of $[Ca^{2+}]_c$ waves (Jouaville *et al*., 1995; Simpson and Russell, 1996; Hajnóczky *et al*., 1999; Tinel *et al*., 1999). Furthermore, Ca^{2+}-induced Ca^{2+} release can be evoked from mitochondria (Ichas *et al*., 1997), and isolated mitochondria immobilized in agarose gel have been shown to drive [Ca^{2+}] waves (Ichas *et al*., 1997) or modulate [Ca^{2+}] waves initiated by sarcoplasmic reticulum (SR) vesicles (Wussling *et al*., 1999). In addition to the role of mitochondria in the physiological control of energy metabolism and $[Ca^{2+}]_c$, new functions of the mitochondria are emerging in cellular signaling that may involve communication between subsets of mitochondria to achieve progressive spreading of signals throughout the cell.

It has recently been established that release of mitochondrial factors to the cytosol is a fundamental component of the cell death machinery during apoptosis. However, the spatiotemporal organization of mitochondrial signals at the subcellular level remains elusive. In response to many triggers, such as growth factor deprivation, glucocorticoids or cytotoxic agents, mitochondria release cytochrome *c* (cyto *c*), apoptosis-inducing factor, Diablo/Smac and caspase enzymes from the intermembrane space, contributing to the cytosolic caspase activation (for a recent review see Green and Reed, 1998; Alnemri, 1999; Bernardi *et al*., 1999; Gross *et al*., 1999; Vander Heiden and Thompson, 1999; Waterhouse and Green, 1999; Desagher and Martinou, 2000; Halestrap *et al*., 2000; Kroemer and Reed, 2000). Most of the studies on the release of mitochondrial apoptotic factors were carried out in a population of cells and so failed to address the mechanisms coordinating the function of individual mitochondria. Using cyto *c* fused to green fluorescence protein (GFP) to investigate the subcellular distribution of cyto *c*, two recent studies reported cyto *c* release that involves subsets or the entire population of mitochondria in the cell (Heiskanen *et al*., 1999; Goldstein *et al*., 2000). Cytochrome *c* release exhibited a cell-specific lag time, but once it occurred, the release from mitochondria was rapid and widespread throughout the cell (Goldstein *et al*., 2000). Thus, the trigger of cyto *c* release may appear either abruptly as a global signal in the cell or through local communication between subsets of mitochondria, thereby facilitating the coordinated response by discrete organelles. The latter mechanism would allow for spreading of the signal from foci of excitation into the remainder of the cell and could be particularly useful to expand the local excitation in large cells undergoing apoptosis. The overall aim of the present study was to determine whether communication between mitochondria supports propagation of the apoptotic signal throughout the cell. Provided that the apoptotic signal can be spread by mitochondrial

waves, it is also of great interest to unravel mechanisms that may allow discrete subcellular loci to initiate the waves.

We have recently described that the concurrence of apoptotic agents (C2 ceramide, staurosporine) and mitochondrial [Ca^{2+}] signals driven by the IP_3R rapidly induces apoptosis (Szalai *et al*., 1999). In this paradigm, transitory opening of the mitochondrial permeability transition pore (PTP) precedes the release of cyto *c*, which, in turn, yields caspase activation and nuclear fragmentation. To study subcellular propagation of the apoptotic signal, cardiac myoblasts (H9c2 cells) were differentiated to myotubes that display ryanodine receptor (RyR)-mediated Ca^{2+} signaling (Szalai *et al*., 2000). Since cardiac and skeletal myotubes are large and rich in mitochondria, we reasoned that utilizing intermitochondrial signaling in propagation of the apoptotic signal can be particularly important in these cells. Here we demonstrate that calcium or caffeine treatment of permeabilized myotubes exposed to pro-apoptotic agents (C2 ceramide, C2; ethanol, EtOH) evokes two sequential regenerative Ca^{2+} waves, which differ in lag time, magnitude and propagation rate. The first wave is characterized by lower amplitude and higher rate of propagation, and disappears if the SR had previously been depleted, suggesting that it originates from the SR. The second, delayed wave is accompanied by mitochondrial depolarization and prevented by cyclosporin A (CSA), suggesting that it originates from mitochondria and is due to PTP opening. The latter wave could still be evoked by Ca^{2+} (but not caffeine) after depletion of the SR, and the resulting mitochondrial depolarization could be prevented by overexpression of Bcl-x_L, but not by caspase inhibitors. Cytosolic [Ca^{2+}] and mitochondrial depolarization waves similar to those evoked in permeabilized cells could be elicited in C2-pretreated intact myotubes after initial Ca^{2+} mobilization by concomitant treatment of cells with caffeine and thapsigargin (Tg). The mitochondrial waves still require treatment with apoptotic agents and could be prevented by CSA. Finally, caffeine treatment of C2-pretreated myotubes causes cyto *c* release and caspase activation temporally coupled to mitochondrial depolarization, and followed by complete execution of the apoptotic program. These data establish the concept that intermitochondrial communication represents an effective means to ensure progressive spreading of the apoptotic signal throughout the cell, and in turn to synchronize the mitochondrial phase of apoptosis.

Results and discussion

Mitochondrial Ca^{2+} release wave follows SR Ca^{2+} release wave in permeabilized myotubes exposed to C2

Under physiological conditions, RyR-mediated Ca^{2+}-activated Ca^{2+} release from the SR appears as $[Ca^{2+}]_c$ waves in myotubes (Bers, 1991). We have demonstrated recently that in permeabilized H9c2 cardiac myotubes, RyR activators (caffeine or Ca^{2+}) give rise to repetitive Ca^{2+} waves that propagate to the mitochondria (Hajnóczky *et al*., 2000; Szalai *et al*., 2000). First, we investigated whether RyR-mediated SR Ca^{2+} release waves can also be elicited in permeabilized H9c2 myotubes exposed to apoptotic agents. Figure 1 shows that Ca^{2+} (30 μM $CaCl_2$) induced traveling $[Ca^{2+}]_c$ waves in permeabilized myotubes exposed to C2 (40 μM for 5 min, shown in green). Furthermore, $[Ca^{2+}]_c$ waves were associated with mitochondrial matrix [Ca^{2+}] ($[Ca^{2+}]_m$) increases that followed the spatiotemporal pattern of the $[Ca^{2+}]_c$ waves (shown in red), illustrating the Ca^{2+} signal propagation to the mitochondria. As shown in the graph, [Ca^{2+}] increases were offset in time, but the kinetics of the [Ca^{2+}] rise was relatively constant along the path of wave propagation. On average, these $[Ca^{2+}]_c$ and $[Ca^{2+}]_m$ waves exhibited <10 s lag time, ~20 μm/s propagation rate (Figure 2A) and were very similar to the Ca^{2+}-induced $[Ca^{2+}]_c$ and $[Ca^{2+}]_m$ waves occurring in naive cells (data not shown). Ca^{2+} waves with similar propagation kinetics were also observed in response to another RyR agonist, caffeine (Figure 2A, lower left). These early Ca^{2+} release waves never appeared if the SR Ca^{2+} store was discharged by pretreatment with an inhibitor of the SR Ca^{2+} pumps, Tg (n = 72). Thus, in permeabilized myotubes exposed to apoptotic agents, activation of RyR by Ca^{2+} or caffeine resulted in $[Ca^{2+}]_c$ waves that were relayed to the mitochondria. Based on the constant amplitude and velocity throughout the cell, the RyR-driven $[Ca^{2+}]_c$ waves were propagated by regenerative Ca^{2+} release from the SR.

In naive permeabilized myotubes, the SR-dependent $[Ca^{2+}]_c$ signal gradually decayed, presumably due to sequestration of released Ca^{2+} in the SR and mitochondria (not shown). By contrast, the C2-treated myotubes displayed a second $[Ca^{2+}]_c$ signal (Figure 1, lower panel). The delayed $[Ca^{2+}]_c$ rise also appeared as a wave and duplicated the spatial pattern of the RyR-driven SR Ca^{2+} release wave (compare the green signal exhibited by the two large myotubes in the upper and lower set of images), but the $[Ca^{2+}]_c$ rise was considerably larger (peak $[Ca^{2+}]_c$ during the first and second waves 5.1 ± 1.4 and 28.0 ± 1.4 μM, respectively, n = 47) and displayed slower propagation (lower graph). Using Ca^{2+} (30 μM $CaCl_2$) to evoke RyR activation, the average lag time of the second $[Ca^{2+}]_c$ wave was 422 ± 37 s (n = 37; Figure 2A, right). In sharp contrast to the early, SR Ca^{2+} release waves, the velocity of the delayed waves was <1 μm/s when either Ca^{2+} (30 μM $CaCl_2$) or caffeine was used for activation of the RyR (Figure 2, lower panel, right). The difference between the propagation rates of the early and delayed waves is also underscored by the histograms showing the velocity distribution (Figure 2). Thus, in permeabilized myotubes exposed to C2, activation of RyR resulted in two sequential waves. The second $[Ca^{2+}]_c$ wave reproduced the spatial pattern of the first wave, but displayed larger amplitude and slower propagation. Delayed $[Ca^{2+}]_c$ waves also appeared in cells exposed to another stress factor, EtOH (35 mM for 48 h), but were absent in naive cells imaged for 20–30 min (not shown).

Mitochondria have been reported to display Ca^{2+}-induced Ca^{2+} release (Ichas *et al*., 1997), and exposure to apoptotic agents was found to promote mitochondrial Ca^{2+} release during IP_3R-mediated Ca^{2+} spikes (Szalai *et al*., 1999). Thus, we reasoned that the delayed waves reflected mitochondrial Ca^{2+} release. However, $[Ca^{2+}]_m$ measured with compartmentalized rhod2 showed only a small and gradual decline during the slow $[Ca^{2+}]_c$ waves

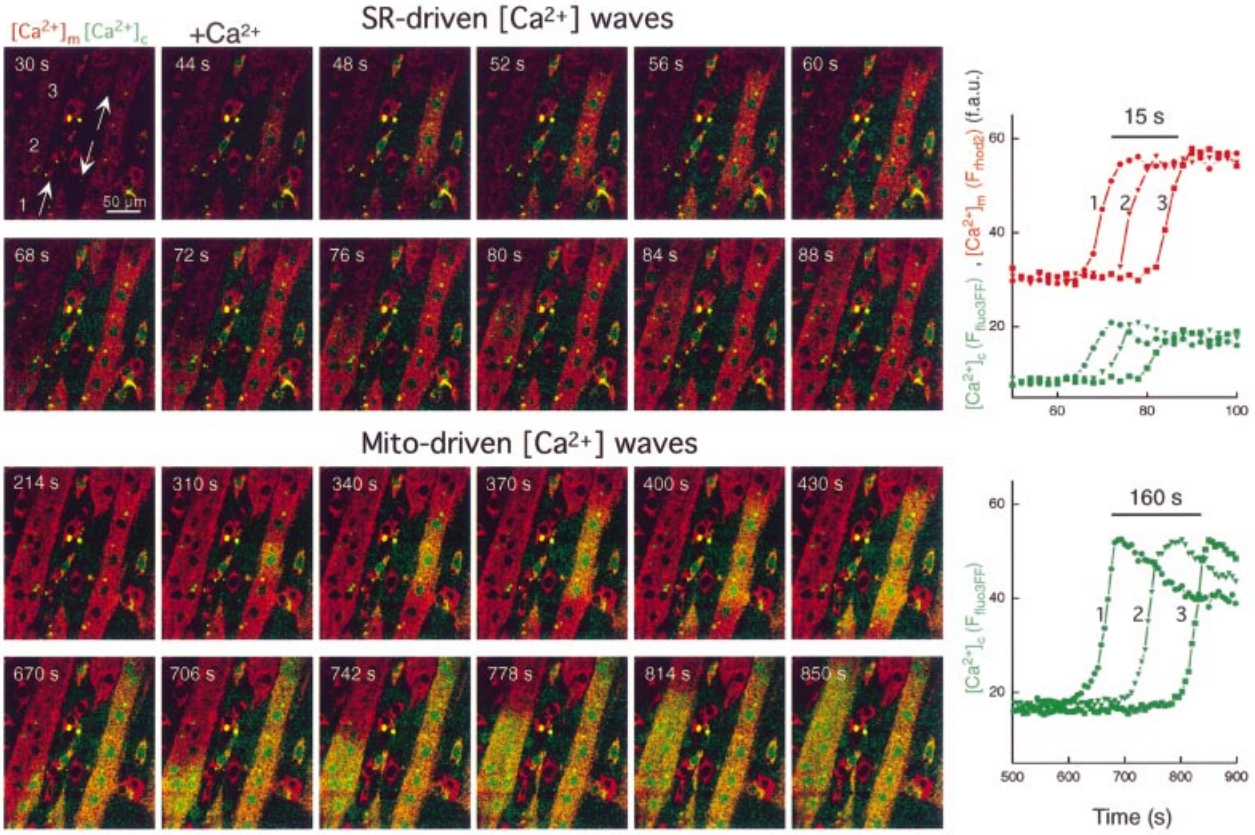

Fig. 1. SR- and mitochondria-driven $[Ca^{2+}]$ waves in C2-pretreated permeabilized cardiac myotubes. Simultaneous confocal imaging of $[Ca^{2+}]_c$ and $[Ca^{2+}]_m$ using fluo3FF added to the incubation medium and compartmentalized rhod2. The upper two rows of $F_{fluo3FF}$ and F_{rhod2} images (presented as green–red overlays) show that Ca^{2+}-induced (30 μM $CaCl_2$) Ca^{2+} release from SR resulted in a $[Ca^{2+}]_c$ wave that was associated with a $[Ca^{2+}]_m$ wave. The upper graph shows corresponding traces of $[Ca^{2+}]_m$ and $[Ca^{2+}]_c$ calculated for three subregions of the cell (marked by numbers, ~30 pixels each) chosen to be in line with the apparent direction of wave propagation. As shown in the lower two rows of images, the first $[Ca^{2+}]_c$ wave was followed by a second $[Ca^{2+}]_c$ wave. Although both $[Ca^{2+}]_c$ waves originated from the same region and exhibited the same propagation pattern, the second wave was ~10 times slower and appeared as a substantially larger $[Ca^{2+}]_c$ increase. The lower graph shows the time course of the mitochondria-driven $[Ca^{2+}]_c$ wave at the subregions shown in the upper panel. Note the different time scales used for presentation of the first and second waves.

(not shown). Importantly, Ca^{2+} release from the mitochondria evoked by uncoupler [1 μM carbonylcyanide-*p*-(trifluoromethoxy)phenylhydrazone (FCCP)] also appeared as a rapid and robust rise in $[Ca^{2+}]_c$ associated with a delayed and relatively small decrease in $[Ca^{2+}]_m$ (not shown). One potential explanation of these results is that compartmentalized rhod2 ($K_d \approx 1$ μM) became saturated with Ca^{2+} accumulated by the mitochondria and, subsequently, during mitochondrial Ca^{2+} release, the robust $[Ca^{2+}]_c$ elevation (28 ± 1.4 μM, see above) sustained the saturated state of rhod2. Thus, we also monitored $[Ca^{2+}]_m$ using a low affinity analog of rhod2, rhod2FF ($K_d \approx 19$ μM). Figure 3 shows that the fluorescence of compartmentalized rhod2FF showed a decrease that appeared as a wave coupled to the second $[Ca^{2+}]_c$ wave. Addition of a Ca^{2+} chelator immediately after the wave evoked a decrease in $F_{rhod2FF}$ and, subsequently, addition of Ca^{2+} caused an increase in $F_{rhod2FF}$, indicating that rhod2FF was not released from the mitochondria during the wave (not shown). Taken together, these data demonstrate a decrease in $[Ca^{2+}]_m$ during the delayed $[Ca^{2+}]_c$ wave, suggesting that mitochondria could serve as a source of the Ca^{2+} release in myotubes exposed to C2. Since Ca^{2+}-induced Ca^{2+} release from the mitochondria can be mediated by opening of the PTP and C2 facilitates activation of PTP by $[Ca^{2+}]_m$ (Ichas *et al*., 1997; Szalai *et al*., 1999), we studied the effect of CSA, an inhibitor of PTP, on the $[Ca^{2+}]_c$ waves. In every myotube exposed to C2 + CSA (1 μM), addition of Ca^{2+} elicited the early RyR-driven $[Ca^{2+}]_c$ wave, whereas no second wave was observed in 30 min (n = 14). Based on these data, the delayed $[Ca^{2+}]_c$ wave results from mitochondrial Ca^{2+} release and is likely to involve activation of PTP.

Coupling of mitochondrial depolarization to the delayed $[Ca^{2+}]_c$ waves in permeabilized myotubes exposed to C2 or EtOH

Opening of PTP results in loss of the mitochondrial membrane potential ($\Delta\Psi_m$). To evaluate the effect of Ca^{2+} pulses on $\Delta\Psi_m$, confocal imaging of tetramethylrhodamine ethyl ester (TMRE)-loaded naive, C2-pretreated (40 μM for 5 min) and EtOH-pretreated (35 mM for 48 h) permeabilized myotubes was used. Prior to Ca^{2+} addition, TMRE fluorescence intensities were similar in naive, C2- and EtOH-pretreated cells (100.4 ± 4.6, 99.6 ± 3.5 and 96.4 ± 4.2 arbitrary units, respectively), suggesting that pre-incubation with C2 or EtOH by itself did not cause mitochondrial depolarization. Ca^{2+} pulses (50 μM $CaCl_2$ each for 10 min) evoked relatively small depolarization in naive cells, whereas Ca^{2+} pulses resulted

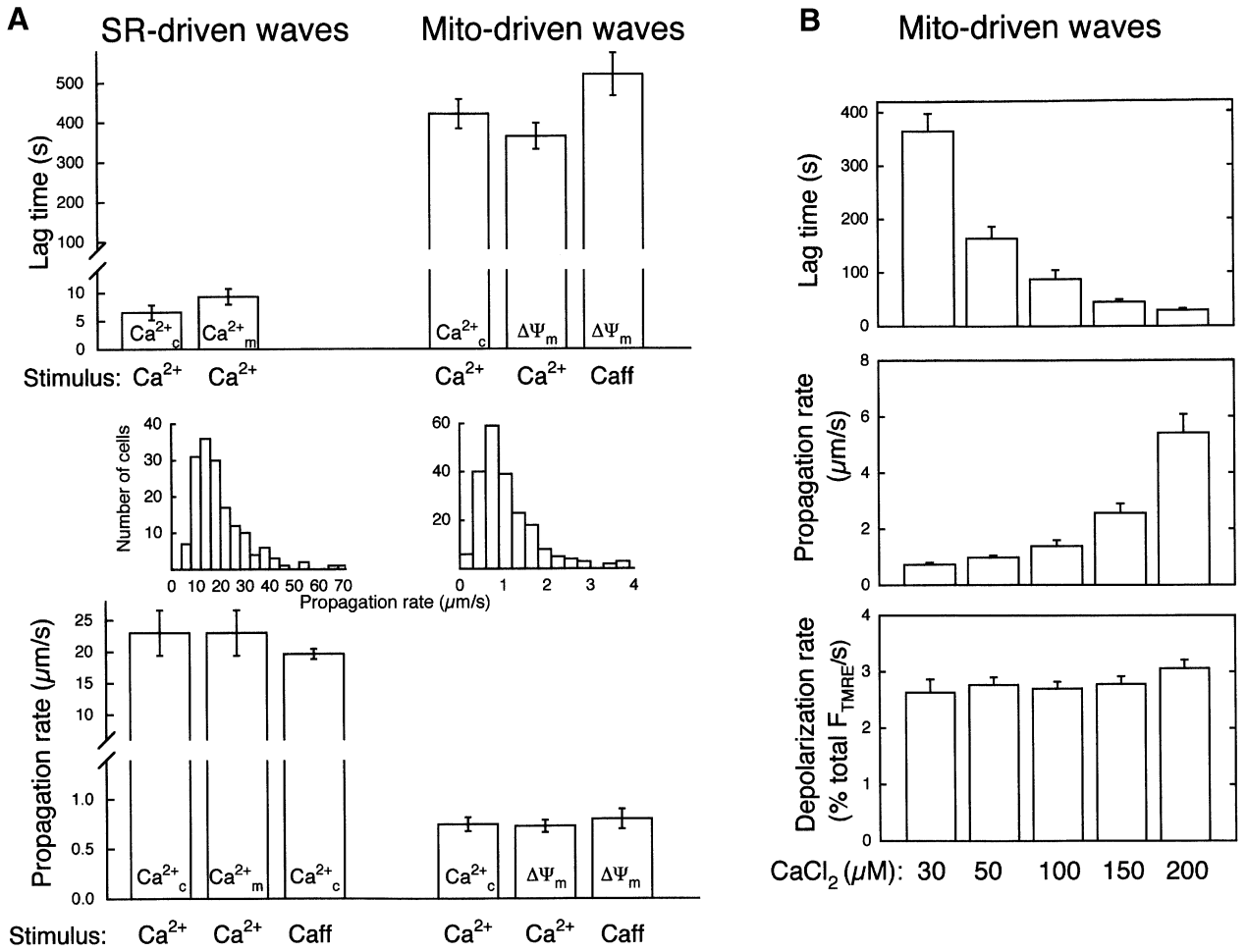

Fig. 2. Kinetic properties of waves originated from SR and mitochondria. (**A**) Comparison of the lag time and propagation rate of waves driven by SR and mitochondria in C2-pretreated permeabilized myotubes. $[Ca^{2+}]$ and $\Delta\Psi_m$ waves were triggered by addition of a Ca^{2+} pulse (30 μM $CaCl_2$) or caffeine (10 mM) and were monitored as described in Figures 1, 4 and 5 (n = 23–162 for each condition). (**B**) Effect of $[Ca^{2+}]_c$ on lag time, propagation rate of $\Delta\Psi_m$ waves and rate of depolarization (n = 40–57). Depolarization rates were normalized to the total ΔF_{TMRE}.

in dissipation of $\Delta\Psi_m$ in C2- and EtOH-pretreated cells (naive 21.2 ± 3.3%, C2 82.7 ± 2.4 and EtOH 73.4 ± 5.3% normalized to the complete depolarization achieved in the presence of uncoupler; p <0.001 for C2 versus naive and EtOH versus naive, n = 18, 24 and 14, respectively).

To evaluate the role of PTP opening in Ca^{2+}-induced depolarization, we studied whether dissipation of $\Delta\Psi_m$ can be inhibited by CSA. CSA (1 μM) did not exert a significant effect on Ca^{2+}-induced changes of $\Delta\Psi_m$ in naive permeabilized cells (n = 4), but inhibited the Ca^{2+}-induced loss of $\Delta\Psi_m$ in cells exposed to C2 or EtOH (n = 5 and n = 7, respectively). FK506 (10 μM), another immunophilin drug, which fails to affect mitochondrial cyclophilin D, did not prevent the loss of $\Delta\Psi_m$ (n = 3; not shown).

Experiments were also carried out to test caffeine-induced $[Ca^{2+}]_c$ and $\Delta\Psi_m$ responses in naive and C2-pretreated permeabilized myotubes. The $[Ca^{2+}]_c$ spikes evoked by caffeine in naive cells were associated with small depolarization (16.6 ± 1.2% decrease in F_{TMRE} in 10 min, n = 65). By contrast, caffeine-induced $[Ca^{2+}]_c$ spikes evoked a substantial decrease in $\Delta\Psi_m$ in C2-pretreated myotubes (46.5 ± 1.9% decrease, n = 62), which was largely inhibited by CSA (1 μM) pretreatment (21.2 ± 3.8% decrease, n = 12). Importantly, the large depolarization in Ca^{2+} + C2-, Ca^{2+} + EtOH- or caffeine + C2-treated cells always followed the RyR-mediated $[Ca^{2+}]_c$ spikes after considerable delay (see below).

Taken together, these data provided evidence that RyR-mediated $[Ca^{2+}]_c$ transients and the ensuing $[Ca^{2+}]_m$ signal can trigger activation of PTP in myotubes exposed to apoptotic stimuli. Apoptotic agents control this process by transforming PTP into a state sensitive to the $[Ca^{2+}]_m$ signals (C2, EtOH, present study; C2, staurosporine, Szalai *et al.*, 1999).

The spatiotemporal pattern of mitochondrial depolarization was studied first by imaging the time course of $\Delta\Psi_m$ at subcellular resolution (Figures 4 and 5). Similarly to the $[Ca^{2+}]_c$ signal, the Ca^{2+}-induced mitochondrial depolarization initiated in discrete subcellular regions and propagated as waves through the myotubes exposed to C2 (Figures 4A and 5) or EtOH (Figure 4B). Depolarization waves could also be induced by caffeine in C2-treated myotubes (Figure 4C). In many myotubes, the intensity of F_{TMRE} exhibited subcellular heterogeneities, which may reflect a heterogeneous population of mitochondria with varying $\Delta\Psi_m$, but the direction of F_{TMRE} gradients did not determine the evolution pattern of the depolarization

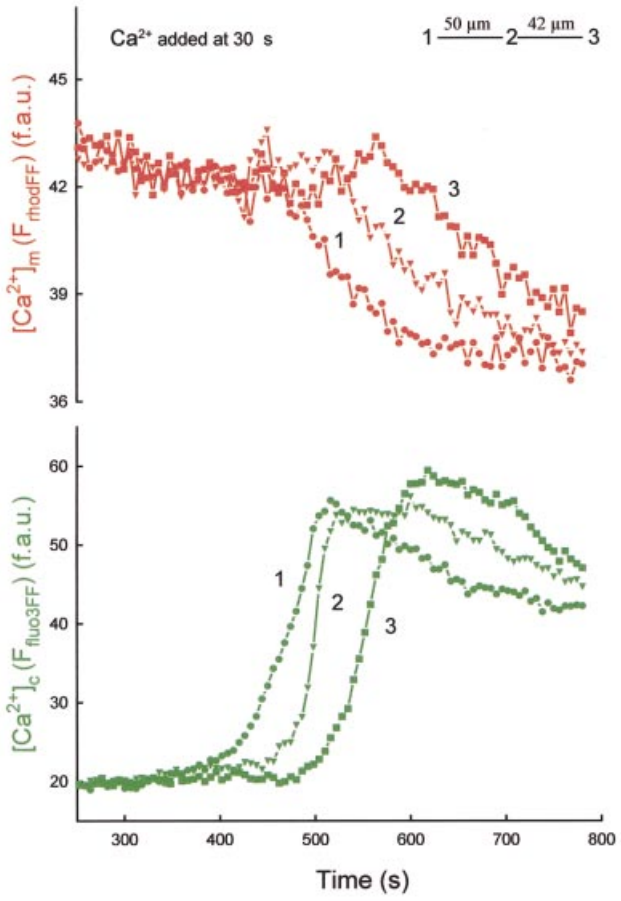

Fig. 3. Decrease in $[Ca^{2+}]_m$ during mitochondria-driven $[Ca^{2+}]_c$ waves. Measurement of $[Ca^{2+}]_m$ was carried out using a low affinity Ca^{2+} tracer, rhod2FF, simultaneously with measurement of $[Ca^{2+}]_c$ using fluo3FF. $[Ca^{2+}]_c$ waves were evoked as described in Figure 1. The graph shows traces of $[Ca^{2+}]_m$ and $[Ca^{2+}]_c$ calculated for three subregions of the cell chosen to be in line with the apparent direction of wave propagation.

waves. For example, in Figure 4A, the wave started from a region displaying relatively bright F_{TMRE}, whereas in Figure 4C the wave initiated from a dark area. The kinetic properties of wave propagation were studied by measuring the time course of fluorescence changes at points along a line parallel to the direction of the waves in each cell. As shown by the traces in Figure 4A and B, depolarization responses were offset, but similar kinetics of mitochondrial depolarization were recorded along the entire path of wave propagation. In addition, a line scan type image was created by selecting a line parallel to the direction of wave propagation, obtaining the corresponding fluorescent signal from every two-dimensional image in the time series and stacking the successive lines horizontally (Figure 4A). This presentation shows that the rate of wave spreading was relatively constant throughout the cell. Since the velocity of the wave and the rate of depolarization do not decline with distance from the site of wave origin, simple diffusion of a messenger is unlikely to account for the wave propagation. By contrast, a regenerative model that includes signaling between neighboring mitochondria may underlie the observed kinetics of the mitochondrial depolarization and delayed $[Ca^{2+}]_c$ waves.

Mechanism of the mitochondrial waves

Consistent with the idea that opening of the PTP caused the mitochondria-driven delayed $[Ca^{2+}]_c$ waves as well as the depolarization waves, the lag time and propagation rate of the depolarization waves evoked by 30 µM $CaCl_2$ were similar to those of the mitochondria-driven $[Ca^{2+}]_c$ waves (Figure 2A). To visualize the spatiotemporal arrangements between mitochondrial Ca^{2+} release waves and depolarization waves, $[Ca^{2+}]_c$ was monitored simultaneously with $\Delta\Psi_m$ using fluo3FF (Figure 5A). These studies revealed that the waves of mitochondrial depolarizations were coupled to waves of $[Ca^{2+}]_c$ elevations. To evaluate the role of the $[Ca^{2+}]_c$ response in the evolution of these waves, we investigated the effect of changes in $[Ca^{2+}]_c$ on wave propagation. As shown in Figure 5A, the evolution of $\Delta\Psi_m$ and $[Ca^{2+}]_c$ waves was interrupted, and partial regeneration of $\Delta\Psi_m$ was observed when a Ca^{2+} chelator, EGTA, was added (n = 10; Figure 5A). Subsequently, the waves resumed and appeared to progress without change in direction when the elevated global $[Ca^{2+}]_c$ was re-established by addition of $CaCl_2$ (Figure 5A). To address the role of mitochondrial Ca^{2+} uptake in wave propagation, an inhibitor of the mitochondrial uptake sites, RuRed, was applied. Figure 5B shows that RuRed arrested propagation of the depolarization wave in C2-pretreated cells (n = 10) and resulted in regeneration of Ψ_m. The $[Ca^{2+}]_c$ wave associated with the depolarization wave was also halted by RuRed (nine out of nine cells, not shown). Importantly, inhibition of wave propagation by RuRed was not due to inhibition of the RyR (see below). As mitochondrial waves were halted immediately by chelation of cytosolic Ca^{2+} or by addition of RuRed, the $[Ca^{2+}]_c$ elevation wave and mitochondrial Ca^{2+} uptake appear to be essential for the wave propagation. Notably, the $[Ca^{2+}]_c$ wave appears to yield a very substantial local $[Ca^{2+}]_c$ rise as the increase in $F_{fluo3FF}$ during the wave is larger than the increase evoked by addition of 50 µM $CaCl_2$ (free $[Ca^{2+}]$ ~15 µM; Figure 5A). The high local $[Ca^{2+}]_c$ may effectively stimulate Ca^{2+} uptake into neighboring mitochondria and this is the step where RuRed may interfere with wave evolution by inhibition of mitochondrial Ca^{2+} accumulation. If mitochondrial Ca^{2+} uptake occurs, elevation of $[Ca^{2+}]_m$ may result in PTP opening and Ca^{2+} release, which subsequently loads up the next group of mitochondria. This Ca^{2+} cycle may serve as a fundamental regenerative mechanism underlying wave propagation. Ca^{2+} preloading of mitochondria adjacent to the wavefront can also explain our observation that the spatial pattern of wave propagation was preserved during treatment with EGTA (Figure 5A).

To understand the machinery of the mitochondrial waves better, the kinetic properties of the depolarization waves were also determined at various global $[Ca^{2+}]_c$. Figure 2B shows that as the amount of added Ca^{2+} was increased: (i) the lag time of the mitochondrial waves decreased and (ii) the propagation rate increased. By contrast, the rate of $\Delta\Psi_m$ loss was not affected by the Ca^{2+} dose (Figure 2B, lower; 2.79 ± 0.07%/s, n = 216). Also, a similar rate was obtained using caffeine to initiate the mitochondrial wave via the SR wave (2.89 ± 0.12%/s,

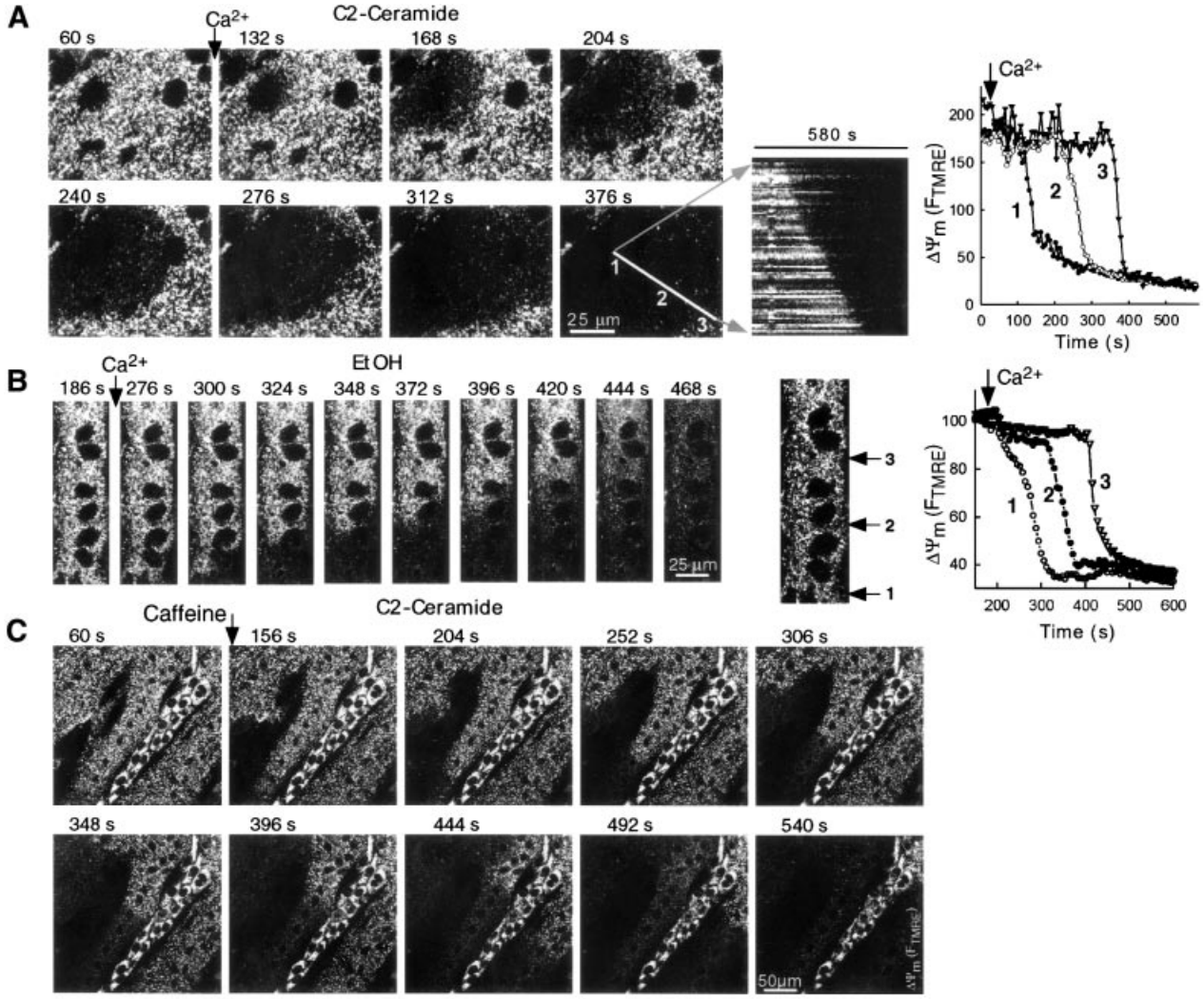

Fig. 4. Waves of Ca^{2+} signal-induced mitochondrial depolarization in permeabilized myotubes exposed to C2 or EtOH. Confocal image time series of TMRE fluorescence show the spatial pattern of depolarization evoked by Ca^{2+} (**A** and **B**; two pulses of 50 µM $CaCl_2$ each) and 10 mM caffeine + 10 µM $CaCl_2$ (**C**) in permeabilized H9c2 myotubes exposed to C2 (A and C; 40 µM for 5 min) or EtOH (B; 35 mM for 48 h). Although caffeine by itself elicited mitochondrial depolarization in C2-pretreated cells (see Results), in the experiments shown in the figures caffeine was added together with 10 µM $CaCl_2$ to optimize Ca^{2+} loading of the intracellular stores. Graphs show time courses of TMRE fluorescence for regions selected along the path of wave propagation (marked with numbers).

n = 32). Shortening of the lag time at higher extramitochondrial $[Ca^{2+}]$ is attributed to the fact that activation of mitochondrial Ca^{2+} uptake sites is more effective as $[Ca^{2+}]_c$ is increased. A substantial increase in the rate of wave propagation would not be expected if Ca^{2+} released from one mitochondrion is taken up by a neighboring one. However, at higher extramitochondrial $[Ca^{2+}]$, the overall mitochondrial Ca^{2+} loading state may be greater before wave initiation, thereby sensitizing the mitochondria, and so less Ca^{2+} uptake is needed during the wave propagation to elicit PTP opening. Nevertheless, once the PTP opens, depolarization occurs independently of the triggering $[Ca^{2+}]_c$.

Anti-apoptotic members of the Bcl-2 family (Bcl-2, Bcl-x_L) have been demonstrated to prevent cyto *c* release (for recent reviews see Green and Reed, 1998; Fadeel *et al*., 1999; Gross *et al*., 1999; Martinou, 1999; Vander Heiden and Thompson, 1999; Waterhouse and Green, 1999; Kroemer and Reed, 2000; Tsujimoto and Shimizu, 2000) and have recently been shown to inhibit PTP (Shimizu *et al*., 1998; Zamzami *et al*., 1998). To determine whether the traveling mitochondrial waves are sensitive to Bcl-x_L, the effect of Bcl-x_L overexpression on Ca^{2+}-induced depolarization waves was investigated. During exposure to C2 + Ca^{2+}, dissipation of $\Delta\Psi_m$ was observed in 94% of the cells expressing GFP by itself (33 out of 35 cells), but in only 8% (4 out of 53 cells) of the cells expressing Bcl-x_L + GFP (calculated as >50% decrease in TMRE fluorescence in 15 min). Traveling waves were observed in almost 89% (176 out of 198 cells) of the non-transfected cells and the cells expressing GFP by itself, whereas only 3% (2 out of 53) of the Bcl-x_L + GFP-overexpressing cells exhibited wave. These results show that Bcl-x_L interferes with the mechanism that underlies the generation of $\Delta\Psi_m$ waves. Recently, Bcl-2/Bcl-x_L has been reported to control the endoplasmic reticulum (ER) as well as the mitochondrial Ca^{2+} store. Although lowering of $[Ca^{2+}]_{ER}$ (Foyouzi-Youssefi *et al*., 2000; Pinton *et al*., 2000) may attenuate the RyR-induced mitochondrial Ca^{2+} load, this

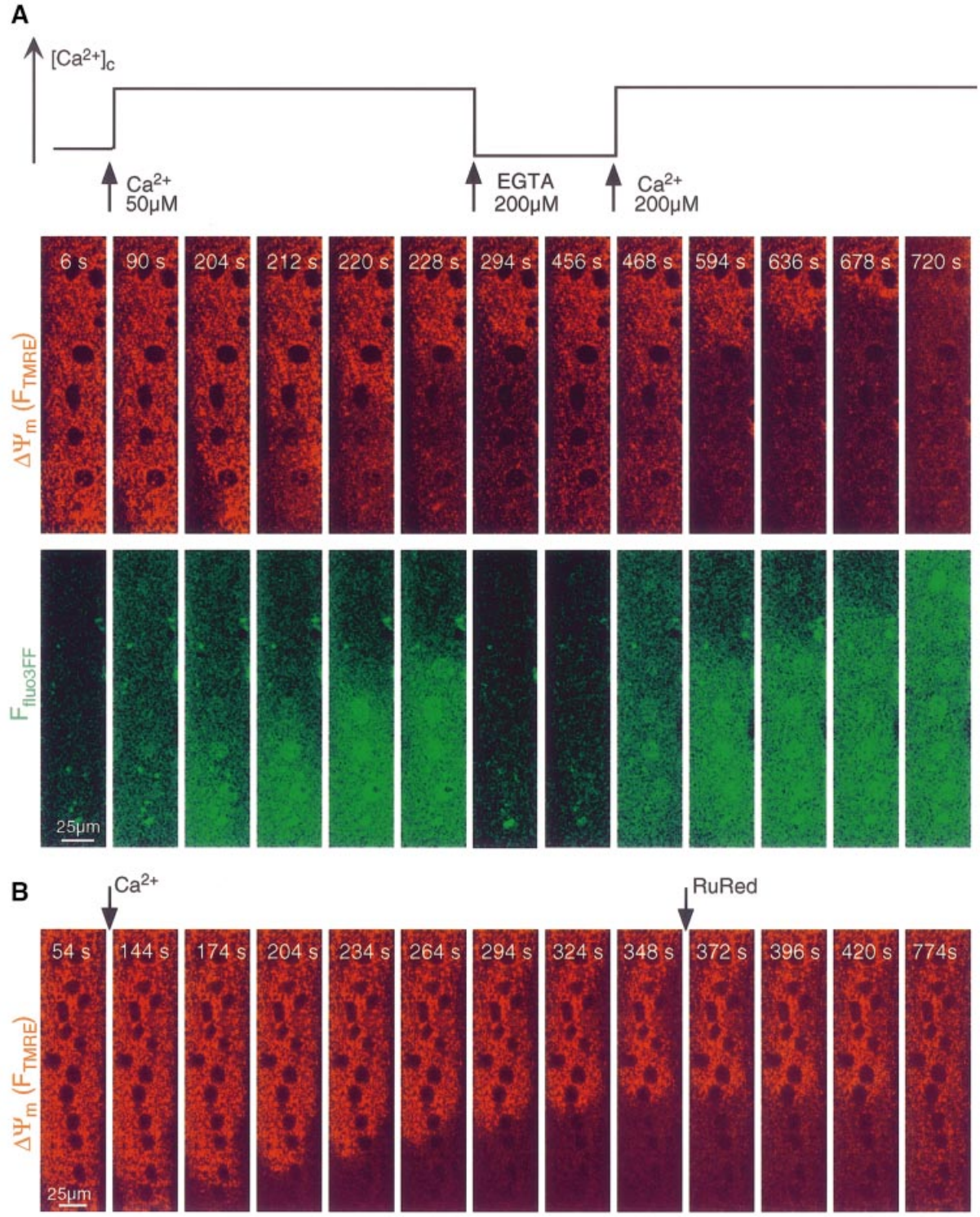

Fig. 5. Mitochondrial depolarization and Ca^{2+} release waves depend on cytosolic $[Ca^{2+}]$ rise and mitochondrial Ca^{2+} uptake. (**A**) Simultaneous confocal imaging of $[Ca^{2+}]_c$ and $\Delta\Psi_m$ carried out in permeabilized H9c2 myotubes. The fluorescence intensities of TMRE and fluo3FF reflecting $\Delta\Psi_m$ and $[Ca^{2+}]_c$ are depicted on linear red and green scales, respectively. Importantly, the fluo3FF confocal images reflect $[Ca^{2+}]_c$ changes in the selected focus plane. Therefore, rapid Ca^{2+} mobilization from intracellular stores is associated with fluo3FF responses even if a global $[Ca^{2+}]_c$ rise does not occur. The plot above the confocal image time series shows the time course profile of global $[Ca^{2+}]$ changes in the cytosolic buffer. Waves were elicited in C2-treated permeabilized cells by addition of 50 µM $CaCl_2$ and subsequently stopped by addition of a Ca^{2+} chelator (200 µM EGTA). When global $[Ca^{2+}]_c$ was increased again, propagation of the waves continued the original spatial pattern. Changes in pH in the incubation medium associated with addition of EGTA and Ca^{2+} were <0.1 units. (**B**) Inhibition of the Ca^{2+}-induced depolarization wave by RuRed (2 µM) in a C2-pretreated permeabilized myotube. Confocal image time series displays TMRE fluorescence on a linear red scale. As this experiment was carried out using cells pretreated with Tg (2 µM) and Ry (200 µM), inhibition of RyR by RuRed did not account for the effect of RuRed on wave propagation.

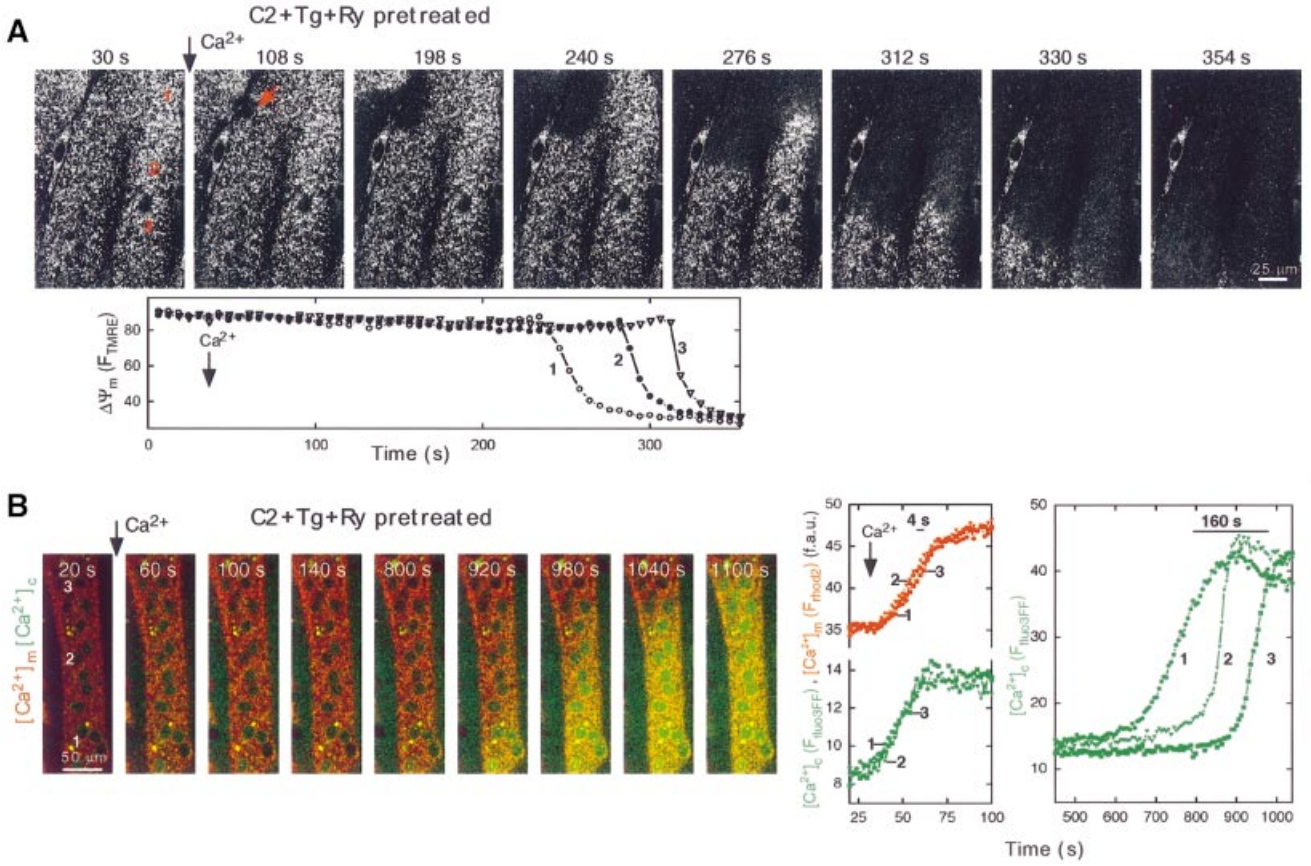

Fig. 6. Mitochondria-driven waves in cells with inhibited SR Ca^{2+} transport. (**A**) Confocal image time series showing a propagating depolarization wave evoked by addition of Ca^{2+} (50 μM $CaCl_2$) in a permeabilized H9c2 cell pretreated with Tg (2 μM) + Ry (200 μM) + C2 (40 μM). The fluorescence intensity of TMRE reflecting $\Delta\Psi_m$ is shown using grayscale. Time courses of the F_{TMRE} changes are shown at three intracellular regions selected along the path of wave propagation. (**B**) Image time series showing a mitochondria-driven $[Ca^{2+}]_c$ wave in a permeabilized myotube pretreated with Tg + Ry + C2. Simultaneous confocal imaging of $[Ca^{2+}]_c$ (green) and $[Ca^{2+}]_m$ (red) was carried out using fluo3FF and compartmentalized rhod2 as described in Figure 5. In contrast to the results shown in Figure 1, addition of Ca^{2+} did not evoke SR-driven waves (images: 60, 100, 140 s and graphs). However, after >10 min lag time, a slowly propagating large amplitude $[Ca^{2+}]_c$ wave appeared, similarly to the mitochondrial wave shown in Figure 5. The right graph shows time courses (green) calculated for the marked subcellular regions.

effect by itself can not account for the protection against mitochondrial waves, since even complete depletion of the ER Ca^{2+} store did not prevent generation of mitochondrial waves in C2-treated cells (see below; Figure 6A and B). Augmented mitochondrial Ca^{2+} uptake capacity and elevated $\Delta\Psi_m$ have also been reported in Bcl-2-overexpressing cells (Murphy *et al*., 1996; Zhu *et al*., 1999), presumably reflecting stabilization of a closed conformation of PTP by Bcl-2/Bcl-x_L. This effect is thought to be particularly important in prevention of the mitochondrial waves by Bcl-x_L. Caspases are activated in a broad range of apoptotic models. In order to determine whether caspase activity was required for wave evolution, experiments were also carried out in the presence of a broad-range caspase inhibitor, z-Val-Ala-Asp-CH_2F (zVAD-FMK; 50 μM). zVAD-FMK failed to prevent the depolarization waves (10 out of 10 cells), suggesting that activation of caspases is not essential for coordination of PTP opening during Ca^{2+} signals in this system.

Initiation of mitochondrial waves

Our results demonstrating the coupling between RyR-driven SR Ca^{2+} release waves and mitochondrial waves (Figure 1) raise the question whether mitochondrial waves can be generated without the contribution of SR Ca^{2+} uptake and release. Autonomous activity of the mitochondria was studied by imaging of $\Delta\Psi_m$ in cells pretreated with Tg (2 μM) to deplete the reticular Ca^{2+} store and with a high dose of ryanodine (Ry; 200 μM) to inhibit the RyR. Under these conditions, caffeine failed to elicit a $[Ca^{2+}]_c$ signal, confirming that the SR Ca^{2+} store had been disabled (not shown). Figure 6A shows that pretreatment with Tg + Ry did not prevent induction of depolarization waves by Ca^{2+} pulsing (45 cells). Notably, the Ca^{2+} addition evoked initial $[Ca^{2+}]_c$ and $[Ca^{2+}]_m$ elevations that were relatively large and appeared throughout the cell at the same time, presumably because Ca^{2+} was not taken up by the SR. This early $[Ca^{2+}]_c$ rise was followed by a slowly propagating $[Ca^{2+}]_c$ wave after several hundred seconds of delay (576 ± 29 s, 72 cells, Figure 6B). Propagation rates of the delayed $[Ca^{2+}]_c$ waves evoked by Ca^{2+} (30 μM $CaCl_2$) in the absence or presence of SR Ca^{2+} transport inhibitors were not different (0.75 ± 0.07 versus 0.79 ± 0.04 μm/s, n = 27 and 57, respectively). Thus, inhibitors of the reticular Ca^{2+} store prevented the SR Ca^{2+} release wave, but failed to abolish evolution of the mitochondrial waves. These results provide evidence that subsets of mitochondria are capable of serving as initiation

sites for propagating waves independently of signals emitted by the SR.

To test whether the spatial pattern of the mitochondrial waves is stable, we designed a repetitive stimulation protocol. The major obstacle with these experiments was that the permeabilized cells have a limited lifetime and so execution of even two cycles of stimulation was difficult in many cells. In 6 out of 12 myotubes that showed complete recovery of $\Delta\Psi_m$ after washout of the first Ca^{2+} pulse, the second Ca^{2+} pulse evoked a wave that repeated the spatial pattern of the first wave (not shown). In the rest of the cells, the waves altered their propagation pattern to a small extent or the second waves moved in exactly the opposite direction to the first one. These results suggest that the mitochondrial wave initiation sites may serve as pacemakers and trigger repetitive waves, but other loci may also drive the waves and the mitochondrial population can propagate the waves in any given direction.

As mitochondrial waves depend on mitochondrial Ca^{2+} uptake, we speculated that the mitochondria competent to act as foci for wave initiation may be in a privileged position to accumulate Ca^{2+}. If SR-driven Ca^{2+} waves preceded the mitochondrial waves, the mitochondrial waves always reproduced the spatial pattern of the RyR-dependent SR Ca^{2+} release waves and concurrent mitochondrial Ca^{2+} uptake waves (as shown in Figure 1), indicating that the mitochondrial waves were initiated by the subsets of mitochondria, which were the first to accumulate Ca^{2+}. The spatial distribution of mitochondrial Ca^{2+} uptake was also studied in cells with inhibited SR Ca^{2+} transport (Tg + Ry pretreatment) by measuring the rate of $[Ca^{2+}]_m$ rise at subcellular resolution. The Ca^{2+} uptake rate in the subsets of mitochondria that subsequently served as initiation site was 139 $\pm$ 12.5% of the rate calculated in other mitochondria (n = 15, p <0.05). This result also supports the idea that the initiation sites are distinguished from the rest of the mitochondria by their larger Ca^{2+} uptake. Importantly, mitochondrial waves appeared only if the cells were also exposed to an apoptotic agent, and sensitization of the mitochondria to Ca^{2+} by a C2-activated mechanism could occur throughout the cell in the present experiments. Provided that sensitization by the apoptotic stress is heterogeneous at the subcellular level, the discrete groups of mitochondria serving as initiation sites can also be determined by the intensity of the local stress. Thus, the spatiotemporal pattern of the RyR-mediated Ca^{2+} release from the SR may control which mitochondria accumulate the most Ca^{2+} and in turn serve as initiation sites for the mitochondrial waves. However, intrinsic properties of the mitochondrial uptake sites and the increase in mitochondrial excitability evoked by the apoptotic agent may also determine the initiation regions of the mitochondrial waves.

Mitochondrial death waves in intact myotubes

Next, we investigated the spatiotemporal organization of the mitochondrial $\Delta\Psi_m$ and Ca^{2+} release responses in intact myotubes (Figure 7A). To ensure that the SR store does not play any role in intracellular Ca^{2+} regulation after the initial Ca^{2+} mobilization, caffeine was added together with Tg. RyR-mediated Ca^{2+} mobilization occurred as a rapid and large increase in $[Ca^{2+}]_c$ in naive as well as in C2-pretreated cells (image 96 s, lower left graph). In naive cells, the initial $[Ca^{2+}]_c$ peak was followed by a slow decay without further increase in the next 60 min and, subsequently, addition of uncoupler elicited a robust increase in $[Ca^{2+}]_c$ (43 cells, not shown). By contrast, in C2-pretreated cells, $[Ca^{2+}]_c$ exhibited a late increase (Figure 7A, lower left graph; 41 out of 43 cells, average lag time 24 $\pm$ 2 min) and uncoupler did not cause further $[Ca^{2+}]_c$ increase (not shown). The image series in Figure 7A shows that the late $[Ca^{2+}]_c$ rise propagated as a wave throughout the C2-pretreated cells. Furthermore, the late $[Ca^{2+}]_c$ increase wave was closely coupled to a wave of mitochondrial depolarization (Figure 7A, shown in red). Prior to stimulation with caffeine, TMRE fluorescence intensities were similar in naive, C2- and C2 + CSA-pretreated intact myotubes (104.1 $\pm$ 3.3, 105.0 $\pm$ 3.0 and 103.1 $\pm$ 3.2 arbitrary units, 29, 43 and 11 cells, respectively). At 50 min after Ca^{2+} mobilization, 95% (41 out of 43) of C2-pretreated myotubes displayed a depolarization wave, resulting in a 66% decrease in average TMRE fluorescence; additionally, in many cells (28 out of 43), the wave was completed in 30 min after Ca^{2+} mobilization. By contrast, in naive and CSA + C2-pretreated intact myotubes, no depolarization waves occurred and only 13 and 11% fluorescence decreases were recorded, respectively. Also, no depolarization wave was found in C2-treated cells in the absence of Ca^{2+} mobilization and if C2-pretreated cells (40 μM for 5 h) were incubated in the absence of C2 for an additional 6 h prior to Ca^{2+} mobilization (15 cells). Consistent with the permeabilized myotube data on mitochondrial waves, the propagation rate of the late depolarization wave was 1.3 $\pm$ 0.1 μm/s and the depolarization rate was 2.7 $\pm$ 0.1%/s (41 cells). Collectively, these data show that Ca^{2+} signals brought about mitochondrial sequestration of Ca^{2+} in intact myotubes. In C2-treated intact myotubes, the mitochondrial Ca^{2+} rise triggered mitochondrial depolarization and Ca^{2+} release waves that exhibit very similar propagation properties to the waves recorded in permeabilized cells.

Ca^{2+} signal-induced cyto c release in C2-pretreated intact myotubes

To evaluate whether the mitochondrial depolarization waves led to changes in the intracellular distribution of cyto *c* in intact myotubes, imaging of cyto *c*–GFP and western blotting of cyto *c* were used. In naive myotubes expressing cyto *c*–GFP, GFP fluorescence was concentrated in the mitochondria and was practically excluded from the nuclear matrix and cytosol, as shown by the presence of small dark areas between the mitochondria (Figure 7B, left). A similar cyto *c*–GFP distribution was observed in myotubes exposed to either C2 or caffeine (bar chart). However, in myotubes treated with C2 + caffeine, GFP fluorescence was also found in the cytosol and nuclear matrix (Figure 7B, right). In cells without major morphological alterations, the mitochondria exhibited brighter fluorescence than the cytosol (upper and middle image), whereas in cells with late apoptotic morphology, the labeling of the mitochondrial structures by cyto *c*–GFP disappeared (lower image). Notably, C2 + Ca^{2+} signal-induced redistribution of cyto *c*–GFP to the cytosol was attenuated in the presence of CSA (Figure 7B, bar chart, p <0.001). Using western blot analysis, the cytosolic component of cyto *c* was also found to be elevated in cells

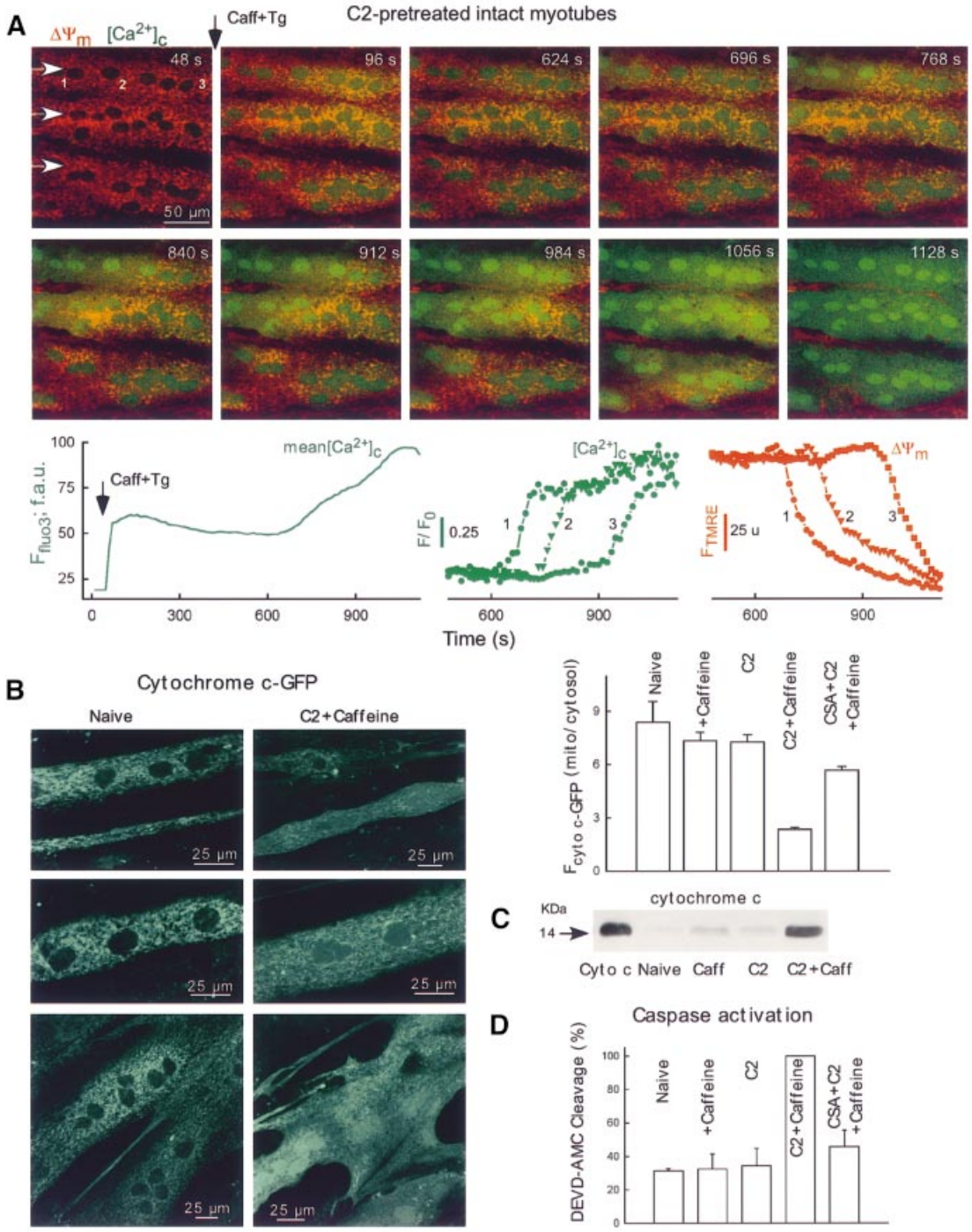

Fig. 7. Mitochondria-driven waves, cyto *c* release and caspase activation in intact myotubes. (**A**) Simultaneous confocal imaging of $[Ca^{2+}]_c$ and $\Delta\Psi_m$ carried out in intact H9c2 myotubes. Fluorescence intensities of TMRE and fluo3 reflecting $\Delta\Psi_m$ and $[Ca^{2+}]_c$ are depicted on linear red and green scales, respectively. Waves were elicited in C2-pretreated cells (40 μM for 5 h) by addition of caffeine (15 mM) and Tg (2 μM). Arrows in the top left panel show the direction of wave propagation. The graphs show the mean time course profile of $[Ca^{2+}]_c$ for the total area of the upper myotube (left) and time courses of $[Ca^{2+}]_c$ (middle) and $\Delta\Psi_m$ (right) at three intracellular regions selected along the path of wave propagation (50 pixels each, marked with numbers). (**B**) Cyto *c*–GFP distribution in intact myotubes. For the experiments shown in (B–D), the adherent myotubes were pre-incubated with C2 (40 μM) or C2 + CSA (1 μM) or solvent for 2 h and, subsequently, 15 mM caffeine or solvent was also added for 4 h. The stimulation protocol is described in detail in Materials and methods. As a quantitative measure of cyto *c*–GFP release, the mean $F_{cyto\ c\text{–}GFP}$ was calculated over the mitochondria and over the nucleus (used to assess cytosolic cyto *c*–GFP) for each cell and the ratios are plotted in the graph (61–191 myotubes). (**C**) Immunoblots showing cyto *c* in cytosol samples generated from intact adherent myotubes treated as described in (B). Cyto c, 14 ng cyto *c*. (**D**) Caspase activity in cytosol samples generated from intact adherent myotubes ($n = 3$).

exposed to C2 + caffeine, whereas incubation of the myotubes with either C2 or caffeine for the same time caused little if any increase (Figure 7C). These data provide further evidence for release of cyto *c*–GFP and cyto *c* from the mitochondria coupled to the mitochondrial depolarization and Ca^{2+} release waves.

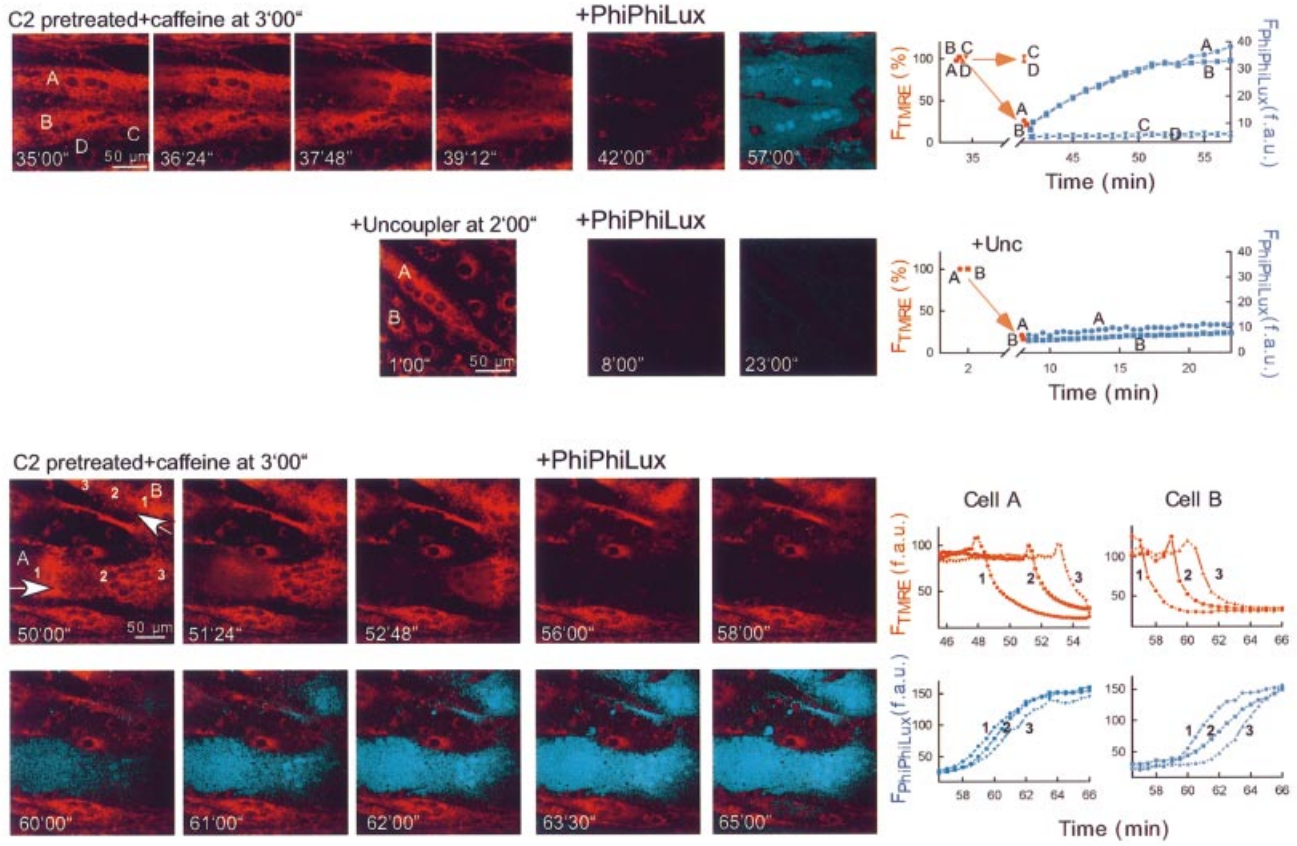

Fig. 8. Mitochondria-driven waves of caspase activation in intact myotubes. Simultaneous imaging of $\Delta\Psi_m$ and fluorescent caspase cleavage products in single intact adherent myotubes treated as described in Figure 7A. After the Ca^{2+} signal-induced depolarization wave or the uncoupler (FCCP 5 μM + oligomycin 10 μg/ml)-induced depolarization was completed, the buffer was replaced with RPMI containing 5 (upper and middle) or 10 μM (lower) cell-permeable fluorogenic caspase substrate (+ PhiPhiLux). Overlaid images of F_{TMRE} (red) and $F_{PhiPhiLux}$ (blue) are shown.

Ca^{2+} signal-induced caspase activation in C2-pretreated intact myotubes

First, caspase activity was monitored in the cytosol harvested from cell populations using Ac-Asp-Gln-Val-Asp-aminomethylcoumarin (DEVD-AMC) cleavage assay. In myotubes exposed to C2 and subsequently to caffeine, higher cytosolic caspase activity was detected than in naive myotubes or in myotubes exposed to C2 or caffeine by itself (Figure 7D, $p < 0.01$). Furthermore, C2 + caffeine-induced caspase activation was attenuated by CSA (Figure 7D, $p < 0.01$).

Subsequently, we established single-cell imaging of caspase cleavage products using a cell-permeable fluorogenic caspase-3 substrate (PhiPhiLux-G_1D_2; Figure 8, upper row). Images of F_{TMRE} show that in response to C2 + caffeine, mitochondrial depolarization occurred in two myotubes (cells A and B), whereas $\Delta\Psi_m$ was not changed in several small cells (e.g. cells C and D). Note that in cells A and B, the mitochondrial depolarization wave was associated with cell contraction, thus resulting in the depolarization wavefront appearing as a bright F_{TMRE} band and with cellular shape change. After addition of caspase substrate, generation of the fluorescent cleavage product was observed in the myotubes displaying mitochondrial depolarization waves (shown in blue in the overlay image; time courses for cells A and B; 34 out of 34 cells), but no change appeared in the non-depolarized cells (e.g. cells C and D; 39 out of 39 cells). Next, we studied whether collapse of $\Delta\Psi_m$ elicited by uncoupler (protonophore) is sufficient to yield rapid cleavage of the caspase substrate (Figure 8, middle row). Uncoupler caused large decreases in F_{TMRE} in every cell, but the increase in PhiPhiLux fluorescence was little if any (<5 unit increase in 39 and <10 unit increase in 6 out of 45 cells in 15 min). These data suggest that the mitochondrial changes associated with depolarization and Ca^{2+} release waves are particularly effective at initiating caspase activation. Simultaneous imaging of TMRE and PhiPhiLux also revealed that caspase cleavage products appear first in the subcellular region where the mitochondrial waves were initiated (Figure 8, lower part). To illustrate this point, the time course of the depolarization wave and increase in PhiPhiLux fluorescence is shown in regions selected along the path of wave propagation in two myotubes (cells A and B). In cell A, the depolarization wave was completed prior to addition of the fluorogenic substrate, whereas in cell B (and in some other elongated cells) the depolarization wave propagated through the cells after addition of the caspase substrate, and the increase in fluorescent cleavage products emerged 2–5 min after depolarization. Of note, the initial upward deflection of the F_{TMRE} traces is due to cell contraction. Thus, the imaging studies provide direct evidence for a close temporal coupling between mitochondrial depolarization/Ca^{2+} release waves and caspase activation. These data also suggest that caspase activation elicited by mitochondrial waves may be controlled

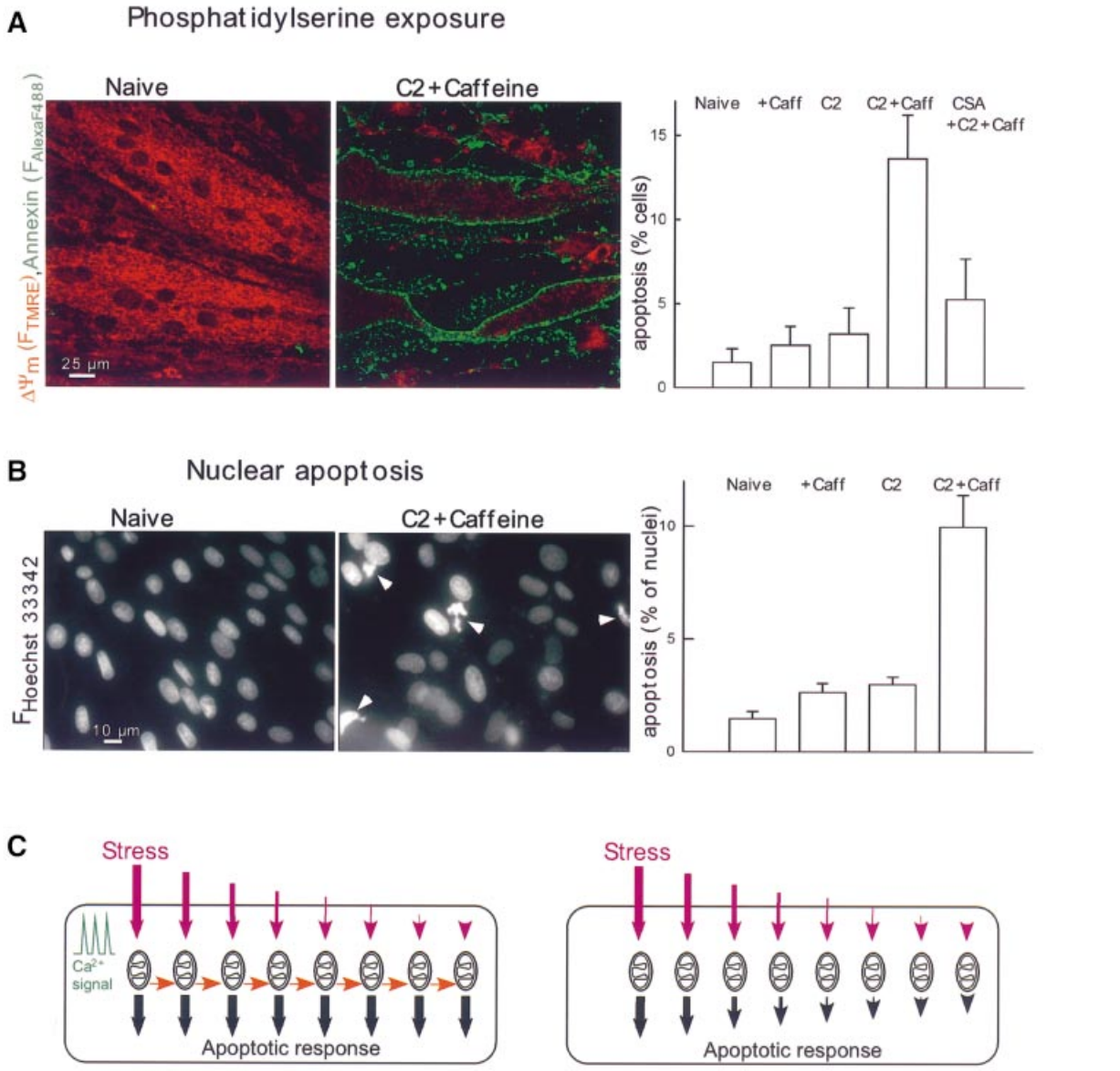

Fig. 9. Ca^{2+} signal-induced apoptosis in C2-pretreated myotubes. (**A**) PS exposure visualized using annexin–Alexa Fluor 488 staining of intact myotubes treated as described in (B) (mean ± SE of values from 1776–2135 myotubes). Note that $\Delta\Psi_m$ was measured simultaneously by annexin staining using TMRE. In myotubes with annexin–Alexa Fluor 488 staining, F_{TMRE} was very low, suggesting large mitochondrial depolarization. (**B**) Nuclear apoptosis detected by staining with Hoechst 33342/propidium iodide (5670–9014 nuclei). Propidium iodide was excluded from >99% of naive, C2-treated and caffeine-stimulated cells and >98% of the C2 + caffeine treated myotubes, suggesting the absence of late apoptotic or necrotic cells. (**C**) Scheme showing how the apoptotic machinery can be controlled by local communication between mitochondria. The predicted responses to a non-uniform stress are shown for mitochondria acting in a coupled manner (left side) or mitochondria activated independently by the apoptotic stress (right side). In both cases, the subsets of mitochondria exposed to vigorous stress respond by rapid and maximal release of apoptotic factors. If these mitochondria also release factors that promote the apoptotic response of neighboring mitochondria (red arrows), apoptotic waves propagate through the cells and the entire mitochondrial population participates in the apoptotic response in a coordinated manner (left panel). By contrast, if there is no lateral signaling between mitochondria, the subsets of mitochondria that experienced less stress give less or slower apoptotic response (right panel).

locally at the subcellular sites of mitochondrial membrane permeabilization.

Ca^{2+} signal-induced apoptosis in C2-pretreated intact myotubes

To determine whether mitochondrial waves and caspase activation are followed by ordered execution of the apoptotic program, phosphatidylserine (PS) exposure was evaluated by annexin staining and nuclear morphology was studied by labeling with Hoechst 33342 and propidium iodide (Figure 9). In myotubes exposed to C2 and subsequently to caffeine, the fraction of cells displaying annexin positivity (Figure 9A, $p < 0.005$, 1776–2530 myotubes) and nuclear condensation was substantially increased (Figure 9B, $p < 0.01$, 5670–9014 nuclei). C2 or caffeine treatment by itself failed to exert a similar effect in 6 h (Figure 9). The effect of C2 + caffeine was attenuated by CSA (Figure 9). Thus, execution of the complete apoptotic program was established by the signaling pathway that utilized mitochondrial excitability and intermitochondrial communication to coordinate activation of the mitochondrial phase of apoptosis throughout the cell.

Apoptotic agents may initiate transformation of mitochondria to an excitable state utilizing a diverse range of molecular mechanisms. A central target of the converging pathways is likely to be Bcl-2/Bcl-x_L. This idea is supported by studies that involved Bcl-2 family proteins as mediators in the pathway from apoptotic stress to cyto *c* release (for a recent review see Green and Reed, 1998; Gross *et al*., 1999; Martinou, 1999; Vander Heiden and Thompson, 1999; Korsmeyer *et al*., 2000; Kroemer and Reed, 2000; Tsujimoto and Shimizu, 2000) and by the present data showing that expression of Bcl-x_L resulted in protection against evolution of the mitochondrial waves. A major mechanism is likely to be that the stress results in a conformational change (e.g. proteolysis, change in the phosphorylation state) of a pro-apoptotic member of the Bcl-x_L family (Bax, Bid, Bad, Bak), which in turn disables a protective function of Bcl-2/Bcl-x_L in the mitochondrial membranes. Considering the numerous regulatory controls exerted on the PTP, this complex by itself may also integrate signals elicited by various stress factors (for a recent review see Kroemer *et al*., 1998; Bernardi *et al*., 1999; Crompton, 1999; Lemasters *et al*., 1999). Although prolonged activation of the signaling pathways that target Bcl-2/Bcl-x_L and PTP may trigger apoptosis independently of changes in $[Ca^{2+}]_m$, synchronization of the mitochondrial phase globally in the cell by $[Ca^{2+}]_m$-driven mitochondrial waves represents a new amplification mechanism that enhances the fidelity of apoptotic signaling. Notably, the environment surrounding the cells in the organisms exhibits dynamic changes in the concentration of stress factors, hormones, growth factors and neurotransmitters. Under these conditions, regenerative signaling mechanisms that propagate the signal at full strength throughout the cell are particularly valuable in determining the fate of the cell.

Release of cyto *c* appears to involve the entire population of mitochondria in the cell (Heiskanen *et al*., 1999; Goldstein *et al*., 2000; an essentially homogeneous release was also observed in the present study). As such, if intermitochondrial communications were not involved in the release of apoptotic factors from the mitochondria, a fully effective apoptotic trigger signal would need to be delivered to every single mitochondrion. This could be difficult in large cells, some of which, such as the myotubes in cardiac or skeletal muscle, are particularly abundant in mitochondria. The high density of mitochondria is apparently a disadvantage if mitochondria should be triggered individually, but it can facilitate spreading of the apoptotic signal if intermitochondrial communication is involved. Moreover, elevation of $[Ca^{2+}]_c$ represents the fundamental signal to initiate each cell contraction in cardiac and skeletal muscle, and so if mitochondria are switched to an excitable state, the Ca^{2+} spikes are available to the mitochondria to initiate apoptotic waves.

The schematic in Figure 9C illustrates how intermitochondrial communication facilitates coordination of the apoptotic response in large cells exposed to a non-uniform stress. In the cell depicted on the left, $[Ca^{2+}]$ spikes trigger apoptotic response of the mitochondria most exposed to stress. The mitochondrial turnover of Ca^{2+} during this process leads to the generation of a lateral signal (red arrows) that recruits the neighboring mitochondria to the apoptotic process. This mechanism results in a regenerative response that spreads throughout the entire mitochondrial population of the cell. Importantly, the large Ca^{2+} signal propagated by the mitochondria may ensure that the mitochondria exposed to a suboptimal stress signal also participate in the coordinated apoptotic response. By contrast, in the absence of the coupling signal, the groups of mitochondria less exposed to stress would produce a smaller or delayed response that may hinder coordinated execution of apoptosis throughout the cell (right).

Conclusions

This study establishes the concept that local communication between mitochondria can ensure propagation of the apoptotic signal throughout the cell. The novel mechanism involves mitochondria releasing activators of the cytosolic components of the apoptotic cascade as well as factors that act on neighboring mitochondria to trigger further release events. This lateral signaling between mitochondria results in a regenerative process that is shown to propagate the apoptotic signal over distances of several hundred micrometers at full strength in a few minutes. Therefore, it appears that this mechanism may be particularly important for coordinated execution of apoptosis in large cells. As a high density of mitochondria facilitates communication between neighboring organelles, the local signaling machinery can be utilized effectively in the large myotubes of heart and skeletal muscle, which are among the cells most abundant in mitochondria.

Materials and methods

Cells

H9c2 cardiac cells (obtained from the American Type Culture Collection) were cultured in Dulbecco's modified essential medium supplemented with 10% (v/v) fetal bovine serum, 2 mM glutamine, 100 U/ml penicillin, 100 μg/ml streptomycin and 1 mM pyruvate in humidified air (5% CO_2) at 37°C. For imaging experiments, cells were plated onto poly-D-lysine-coated glass coverslips. H9c2 myoblasts were grown to reach confluency (1 week in average) and, subsequently, for an additional 5–7 days to allow differentiation to myotubes (Szalai *et al*., 2000).

For measurements of $[Ca^{2+}]_c$ and $\Delta\Psi_m$ in intact myotubes, the cells were pretreated with 40 μM C2 [dissolved in dimethylsulfoxide (DMSO)] for ~5 h prior to addition of caffeine. For the cyto *c* western blot, caspase assay, annexin and Hoechst 33342/propidium iodide staining, 40 μM C2 was present for 6 h and caffeine was added 2 h after C2 addition. To obtain a caffeine-induced $[Ca^{2+}]_c$ rise in most of the myotubes, extracellular Ca^{2+} was increased to 5 mM and depolarization (20 mM KCl) was applied for 10 min. High Ca^{2+} and KCl were washed out 10–20 min before addition of caffeine. This protocol is thought to facilitate RyR-mediated Ca^{2+} release by optimizing the SR Ca^{2+} load (Lukyanenko *et al*., 1999). Permeabilized cells were exposed to 40 μM C2 (dissolved in DMSO) for 5 min prior to addition of Ca^{2+} and ceramide was also present during the entire experiments. Pre-incubation with 35 mM EtOH was for 48 h, and it was not present during measurements.

Prior to use, the cells were pre-incubated for 30 min in an extracellular-like medium (ECM) composed of 121 mM NaCl, 5 mM $NaHCO_3$, 10 mM Na–HEPES, 4.7 mM KCl, 1.2 mM KH_2PO_4, 1.2 mM $MgSO_4$, 2 mM $CaCl_2$, 10 mM glucose and 2% bovine serum albumin (BSA) pH 7.4 at 37°C.

Transfection

After replacement of culture medium by serum-free Opti-MEM (Life Technologies, Inc.), cells were transfected using plasmid DNA [cyto *c*–GFP (Heiskanen *et al*., 1999) and Bcl-x_L (Holinger *et al*., 1999)] and cationic lipid Lipofecta-AMINE or Lipofecta-AMINE 2000 according to the manufacturer's instructions. In the studies of Bcl-x_L-overexpressing myotubes, the cells were co-transfected with plasmid DNA encoding GFP and only green cells were analyzed in the imaging experiments. After 5 h, the cells were placed in a normal growth medium. Imaging was carried out 4–6 days after transfection.

Confocal imaging of $[Ca^{2+}]_c$ simultaneously with $[Ca^{2+}]_m$ in permeabilized myotubes

Cells were loaded with 4 μM rhod2/AM or rhod2FF/AM in ECM in the presence of 0.003% (w/v) pluronic acid at 37°C for 50 min (Csordás *et al*., 1999; Szalai *et al*., 2000). Dye-loaded cells were washed with Ca^{2+}-free buffer composed of 120 mM NaCl, 20 mM Na–HEPES, 5 mM KCl, 1 mM KH_2PO_4, 100 μM EGTA/Tris pH 7.4 and then permeabilized by incubation for 4 min with 15–20 μg/ml digitonin in an intracellular-like medium (ICM) composed of 120 mM KCl, 10 mM NaCl, 1 mM KH_2PO_4, 20 mM Tris–HEPES, 2 mM MgATP pH 7.2 supplemented with 1 μg/ml each of antipain, leupeptin and pepstatin. All the measurements were carried out in the presence of 2 mM MgATP and an ATP-regenerating system composed of 5 mM phosphocreatine, 5 U/ml creatine kinase. Mitochondria were energized with 1 mM malate/5 mM glutamate (complex I substrate) and 2.5 μg/ml oligomycin was also added to prevent reversed function of the mitochondrial H^+ ATPase. ICM was passed through a Chelex column to lower the ambient $[Ca^{2+}]$. Medium free $[Ca^{2+}]$ was <100 nM after Chelex treatment and did not exceed 250–350 nM after addition of ATP, mitochondrial substrates and protease inhibitors. In most of the experiments, 20 μM EGTA was also present during permeabilization to maintain $[Ca^{2+}]$ at 20–50 nM. After permeabilization, the cells were washed into fresh buffer without digitonin and incubated in the imaging chamber at 35°C. To monitor $[Ca^{2+}]_c$, 5 μM fluo3FF was added to the bathing medium after cell permeabilization. The bath volume was 1 ml. To make additions, 200–300 μl of medium were taken out, mixed with the stimulus, returned to the chamber and resuspended with two strokes.

Confocal imaging was carried out using a Bio-Rad MRC1024/2P imaging system equipped with a Kr/Ar-ion laser source (488 and 568 nm excitation) fitted to an Olympus IX70 inverted microscope. Images were captured using 40× UApo and 60× PlanApo objectives. The pixel size was between 0.532 and 0.266 μm, and the axial resolution was ~1 μm. rhod2 and rhod2FF were excited at 568 nm, and fluo3FF at 488 nm. Images were collected every 2 and 6 s for SR- and mitochondria-driven Ca^{2+} waves, respectively. To quantitate responses of individual cells, whole cell areas were masked, whereas to evaluate time courses at subcellular resolution, intracellular regions (30–50 pixels each) were selected along the path of wave propagation. Wave rates were calculated by measuring the time offset in the rising phase of $[Ca^{2+}]_c$ or $[Ca^{2+}]_m$ at half-peak height over known distances within individual myotubes. In many myotubes, the Ca^{2+} signal was associated with cell contraction (e.g. Figure 8, lower images). To make sure that the fluorescence changes were not due to cell contraction, we checked the position of the cells at the beginning as well as at the end of every imaging measurement. Furthermore, in most experiments, two fluorophores were monitored simultaneously, and by evaluation of both signals we could determine the position of the myotubes throughout the experiments.

In confocal imaging measurements of $[Ca^{2+}]_c$ in permeabilized myotubes, the steady-state fluorescence increase displayed by fluo3FF is usually higher in the cellular areas than in cell-free regions (42% difference in the experiment shown in Figure 1). One explanation is that fluo3FF exhibits a higher concentration in the vicinity of cellular membranes and also in the nuclear matrix. Alternatively, the Ca^{2+}-induced increase in fluo3FF fluorescence is promoted by the intracellular environment. Based on the pharmacological profiles, compartmentalization of fluo3FF in the SR or mitochondria is unlikely.

Using a $[Ca^{2+}]$ calibration buffer series (Calcium Calibration Kits #2&3; Molecular Probes), the K_d of fluo3FF for Ca^{2+} was 16 μM at 35°C and pH 7.2. Consistent with this result, the K_d was estimated to be ~16 μM in the intracellular medium measuring the fluo3FF fluorescence at different $[Ca^{2+}]$ concentrations, which were calibrated using other fluorescent Ca^{2+} probes (fura2, rhod2) or calculated using constants as described previously. We carried out *in situ* calibration of fluo3FF in the confocal imaging of $[Ca^{2+}]_c$ in permeabilized myotubes and during the SR Ca^{2+} release wave. The peak value was 5.15 ± 0.3 μM (n = 47), whereas during the mitochondrial wave the peak was 28 ± 1.4 μM (n = 47). In these studies, fluo3FF is likely to respond to rapid changes in $[Ca^{2+}]$ adjacent to cellular membranes and so the $[Ca^{2+}]_{fluo3FF}$ peaks at a somewhat higher concentration than the global $[Ca^{2+}]_c$.

Imaging of $\Delta\Psi_m$ simultaneously with $[Ca^{2+}]_c$ in permeabilized H9c2 myotubes

Cells were loaded with 80 nM TMRE in ECM in the presence of 0.003% (w/v) pluronic acid at 37°C for 15 min. TMRE (10 nM) was also present in the medium during the measurements. Cell permeabilization and incubation were carried as described above. To monitor $[Ca^{2+}]_c$, 5 μM fluo3FF was added to the bathing medium after cell permeabilization. Confocal imaging was carried out using the system described above. TMRE was excited at 568 nm and fluo3FF at 488 nm. Wave rates were calculated by measuring the time offset in either the falling phase of $\Delta\Psi_m$ or the rising phase of $[Ca^{2+}]_c$ at half-peak height over known distances within individual myotubes.

Confocal imaging of $\Delta\Psi_m$ simultaneously with $[Ca^{2+}]_c$ in intact myotubes

Cells were loaded with 5 μM fluo3/AM and 50 nM TMRE in the presence of 0.003% (w/v) pluronic acid at room temperature for 25 and 15 min, respectively. Experiments were performed in ECM containing 0.25% BSA at 35°C. TMRE was excited at 568 nm and fluo3 at 488 nm. In intact cells, the fluorescence of fluo3 was not calibrated in terms of $[Ca^{2+}]_c$ since calibration of a non-ratiometric dye in the cells is difficult. Assuming that the resting $[Ca^{2+}]_c$ was 150 nM and the K_d of fluo3 for Ca^{2+} was 0.81 μM in the cytosol (Thomas *et al*., 2000), the SR- and mitochondria-driven $[Ca^{2+}]_c$ waves peak at ~1 and 5 μM, respectively.

Imaging of cyto c–GFP distribution in intact myotubes

Confocal imaging of intact myotubes expressing cyto *c*–GFP was carried out using the system described above. GFP was excited at 488 nm. To quantitate cyto *c*–GFP release, the mean $F_{cyto\ c\text{–}GFP}$ was calculated over the brightest mitochondrial region (30–50 square pixel area) and over the nucleus (total nuclear area; used to assess cytosolic cyto *c*–GFP) for each cell.

Imaging of caspase products simultaneously with $\Delta\Psi_m$ in intact myotubes

To measure caspase-3(-like) activity, the TMRE-loaded myotubes were incubated with 5–10 μM fluorogenic caspase-3 substrate (PhiPhiLux-G_1D_2; Alexis). Imaging experiments were performed in RPMI. Confocal imaging was carried out using the system described above. TMRE was excited at 568 nm and PhiPhiLux at 488 nm. To quantitate changes in PhiPhiLux fluorescence, the image series was background subtracted and total cell areas or intracellular regions were masked as described above.

Imaging of PS and nuclei in H9c2 myotubes

To evaluate PS exposure, the cells were labeled with annexin–Alexa Fluor 488 (Molecular Probes) according to the manufacturer's instructions. In order to visualize apoptotic and necrotic myotubes, labeling of the cells with 10 μg/ml Hoechst 33342 for 5 min was carried out and 1 μg/ml propidium iodide was present during fluorescence imaging (Szalai *et al*., 1999). Fluorescence images of Hoechst 33342 (excitation 340 nm) and propidium iodide (excitation 545 nm) were collected using a cooled CCD imaging system equipped with a multi-wavelength beamsplitter/emission filter combination as described previously (Szalai *et al*., 1999).

Experiments were carried out with at least three different cell preparations, and 3–8 myotubes were monitored in each experiment. Experimental test conditions were always compared with controls obtained from the same cell culture. The data are shown as mean ± SE. The significance of differences from the relevant controls was calculated by Student's *t*-test.

Western blot analysis and caspase assay in cytosol samples generated from intact myotubes

Myotubes were harvested from 25 cm^2 flasks and permeabilized in ICM using 20 μg/ml digitonin at 37°C for 8 min. Samples were then centrifuged (14 000 *g* for 6 min) and the supernatants were used to measure cytosolic cyto *c* and caspase activity. Western blotting of cyto *c* in cytosol fractions from H9c2 myotubes (25 μg protein each) was carried out as described previously (Szalai *et al*., 1999), except that the proteins were transferred to nitrocellulose membrane and the monoclonal cyto *c* antibody (7H8.2C12) was obtained from PharMingen. DEVD-AMC cleavage was measured as described previously (Szalai *et al*., 1999). Briefly, 180 μl of extract (protein concentration 0.6–1.0 mg/ml) were pre-incubated for 10 min at 35°C and subsequently added to 1420 μl of assay buffer (10% w/v sucrose, 0.1% w/v CHAPS, 5 mM dithiothreitol, 100 mM Tris–HEPES pH 7.2). Assay mixture was incubated in the presence of 12.5 μM DEVD-AMC for 30 min at 35°C and the fluorescence of free aminomethylcoumarin (excitation 350 nm, emission 460 nm) was monitored using a fluorimeter.

Acknowledgements

We thank Drs P.Bernardi, G.Fiskum, J.B.Hoek, J.J.Lemasters, J.Pastorino, E.Rubin and A.P.Thomas for valuable discussions, and Drs X.Lin, M.Madesh and C.J.Buzas for their help with biochemistry. We are indebted to Drs K.M.Heiskanen, M.Bhat, A.-L.Nieminen, E.Holinger, R.Lutz, T.Balla and P.Varnai for plasmid DNA. This work was supported by grants from the NIH and American Heart Association (to G.H.). G.H. is a recipient of a Burroughs Wellcome Fund Career Award. P.P. is a recipient of a Juvenile Diabetes Foundation Postdoctoral Fellowship.

References

Alnemri,E.S. (1999) Hidden powers of the mitochondria. *Nature Cell Biol.*, **1**, 40–42.

Bernardi,P., Scorrano,L., Colonna,R., Petronilli,V. and Di Lisa,F. (1999) Mitochondria and cell death. Mechanistic aspects and methodological issues. *Eur. J. Biochem.*, **264**, 687–701.

Berridge,M.J. (1997) The AM and FM of calcium signalling. *Nature*, **386**, 759–760.

Berridge,M.J., Bootman M.D. and Lipp,P. (1998) Calcium—a life and death signal. *Nature*, **395**, 645–648.

Bers,D.M. (1991) *Excitation–Contraction Coupling and Cardiac Contractile Force*. Kluwer Academic, Dordrecht, The Netherlands, pp. 1–258.

Clapham,D.E. and Sneyd,J. (1995) Intracellular calcium waves. *Adv. Second Messenger Phosphoprotein Res.*, **30**, 1–24.

Crompton,M. (1999) The mitochondrial permeability transition pore and its role in cell death. *Biochem. J.*, **341**, 233–249.

Csordás,G., Thomas,A.P. and Hajnóczky,G. (1999) Quasi-synaptic calcium signal transmission between endoplasmic reticulum and mitochondria. *EMBO J.*, **18**, 96–108.

Desagher,S. and Martinou,J.C. (2000) Mitochondria as the central control point of apoptosis. *Trends Cell Biol.*, **10**, 369–377.

Fadeel,B., Zhivotovsky,B. and Orrenius,S. (1999) All along the watchtower: on the regulation of apoptosis regulators. *FASEB J.*, **13**, 1647–1657.

Foyouzi-Youssefi,R., Arnaudeau,S., Borner,C., Kelley,W.L., Tschopp,J., Lew,D.P., Demaurex,N. and Krause,K.H. (2000) Bcl-2 decreases the free Ca^{2+} concentration within the endoplasmic reticulum. *Proc. Natl Acad. Sci. USA*, **97**, 5723–5728.

Goldstein,J.C., Waterhouse,N.J., Juin,P., Evan,G.I. and Green,D.R. (2000) The coordinate release of cytochrome *c* during apoptosis is rapid, complete and kinetically invariant. *Nature Cell Biol.*, **2**, 156–162.

Green,D.R. and Reed,J.C. (1998) Mitochondria and apoptosis. *Science*, **281**, 1309–1312.

Gross,A., McDonnell,J.M. and Korsmeyer,S.J. (1999) BCL-2 family members and the mitochondria in apoptosis. *Genes Dev.*, **13**, 1899–1911.

Hajnóczky,G., Robb-Gaspers,L.D., Seitz,M.B. and Thomas,A.P. (1995) Decoding of cytosolic calcium oscillations in the mitochondria. *Cell*, **82**, 415–424.

Hajnóczky,G., Hager,R. and Thomas,A.P. (1999) Mitochondria suppress local feedback activation of inositol 1,4,5-trisphosphate receptors by Ca^{2+}. *J. Biol. Chem.*, **274**, 14157–14162.

Hajnóczky,G., Csordas,G., Madesh,M. and Pacher,P. (2000) The machinery of local Ca^{2+} signalling between sarco-endoplasmic reticulum and mitochondria. *J. Physiol.*, **529**, 69–81.

Halestrap,A.P., Doran,E., Gillespie,J.P. and O'Toole,A. (2000) Mitochondria and cell death. *Biochem. Soc. Trans.*, **28**, 170–177.

Heiskanen,K.M., Bhat,M.B., Wang,H.W., Ma,J. and Nieminen,A.L. (1999) Mitochondrial depolarization accompanies cytochrome *c* release during apoptosis in PC6 cells. *J. Biol. Chem.*, **274**, 5654–5658.

Holinger,E.P., Chittenden,T. and Lutz,R.J. (1999) Bak BH3 peptides antagonize Bcl-x_L function and induce apoptosis through cytochrome *c*-independent activation of caspases. *J. Biol. Chem.*, **274**, 13298–13304.

Ichas,F., Jouaville,L.S. and Mazat,J.P. (1997) Mitochondria are excitable organelles capable of generating and conveying electrical and calcium signals. *Cell*, **89**, 1145–1153.

Jouaville,L.S., Ichas,F., Holmuhamedov,E.L., Camacho,P. and Lechleiter,J.D. (1995) Synchronization of calcium waves by mitochondrial substrates in *Xenopus laevis* oocytes. *Nature*, **377**, 438–441.

Korsmeyer,S.J., Wei,M.C., Saito,M., Weiler,S., Oh,K.J. and Schlesinger,P.H. (2000) Pro-apoptotic cascade activates BID, which oligomerizes BAK or BAX into pores that result in the release of cytochrome *c*. *Cell Death Differ.*, **7**, 1166–1173.

Kroemer,G. and Reed,J.C. (2000) Mitochondrial control of cell death. *Nature Med.*, **6**, 513–519.

Kroemer,G., Dallaporta,B. and Resche-Rigon,M. (1998) The mitochondrial death/life regulator in apoptosis and necrosis. *Annu. Rev. Physiol.*, **60**, 619–642.

Lechleiter,J.D., John,L.M. and Camacho,P. (1998) Ca^{2+} wave dispersion and spiral wave entrainment in *Xenopus laevis* oocytes overexpressing Ca^{2+} ATPases. *Biophys. Chem.*, **72**, 123–129.

Lemasters,J.J., Qian,T., Bradham,C.A., Brenner,D.A., Cascio,W.E., Trost,L.C., Nishimura,Y., Nieminen,A.L. and Herman,B. (1999) Mitochondrial dysfunction in the pathogenesis of necrotic and apoptotic cell death. *J. Bioenerg. Biomembr.*, **31**, 305–319.

Lukyanenko,V., Subramanian,S., Gyorke,I., Wiesner,T.F. and Gyorke,S. (1999) The role of luminal Ca^{2+} in the generation of Ca^{2+} waves in rat ventricular myocytes. *J. Physiol.*, **518**, 173–186.

Martinou,J.C. (1999) Apoptosis. Key to the mitochondrial gate. *Nature*, **399**, 411–412.

Meyer,T. (1991) Cell signaling by second messenger waves. *Cell*, **64**, 675–678.

Murphy,A.N., Bredesen,D.E., Cortopassi,G., Wang,E. and Fiskum,G. (1996) Bcl-2 potentiates the maximal calcium uptake capacity of neural cell mitochondria. *Proc. Natl Acad. Sci. USA*, **93**, 9893–9898.

Pinton,P., Ferrari,D., Magalhaes,P., Schulze-Osthoff,K., Di Virgilio,F., Pozzan,T. and Rizzuto,R. (2000) Reduced loading of intracellular Ca^{2+} stores and downregulation of capacitative Ca^{2+} influx in Bcl-2-overexpressing cells. *J. Cell Biol.*, **148**, 857–862.

Romashko,D.N., Marban,E. and O'Rourke,B. (1998) Subcellular metabolic transients and mitochondrial redox waves in heart cells. *Proc. Natl Acad. Sci. USA*, **95**, 1618–1623.

Shimizu,S., Eguchi,Y., Kamiike,W., Funahashi,Y., Mignon,A., Lacronique,V., Matsuda,H. and Tsujimoto,Y. (1998) Bcl-2 prevents apoptotic mitochondrial dysfunction by regulating proton flux. *Proc. Natl Acad. Sci. USA*, **95**, 1455–1459.

Simpson,P.B. and Russell,J.T. (1996) Mitochondria support inositol 1,4,5-trisphosphate-mediated Ca^{2+} waves in cultured oligodendrocytes. *J. Biol. Chem.*, **271**, 33493–33501.

Szalai,G., Krishnamurthy,R. and Hajnóczky,G. (1999) Apoptosis driven by IP(3)-linked mitochondrial calcium signals. *EMBO J.*, **18**, 6349–6361.

Szalai,G., Csordás,G., Hantash,B., Thomas,A.P. and Hajnóczky,G. (2000) Calcium signal transmission between ryanodine receptors and mitochondria. *J. Biol. Chem.*, **275**, 15305–15313.

Thomas,A.P., Bird,G.S., Hajnóczky,G., Robb-Gaspers,L.D. and Putney,J.W.,Jr (1996) Spatial and temporal aspects of cellular calcium signaling. *FASEB J.*, **10**, 1505–1517.

Thomas,D., Tovey,S.C., Collins,T.J., Bootman,M.D., Berridge,M.J. and Lipp,P. (2000) A comparison of fluorescent Ca^{2+} indicator properties and their use in measuring elementary and global Ca^{2+} signals. *Cell Calcium*, **28**, 213–223.

Tinel,H., Cancela,J.M., Mogami,H., Gerasimenko,J.V., Gerasimenko, O.V., Tepikin,A.V. and Petersen,O.H. (1999) Active mitochondria surrounding the pancreatic acinar granule region prevent spreading of inositol trisphosphate-evoked local cytosolic Ca^{2+} signals. *EMBO J.*, **18**, 4999–5008.

Tsujimoto,Y. and Shimizu,S. (2000) Bcl-2 family: life-or-death switch. *FEBS Lett.*, **466**, 6–10.

Vander Heiden,M.G. and Thompson,C.B. (1999) Bcl-2 proteins: regulators of apoptosis or of mitochondrial homeostasis? *Nature Cell Biol.*, **1**, E209–E216.

Waterhouse,N.J. and Green,D.R. (1999) Mitochondria and apoptosis: HQ or high-security prison? *J. Clin. Immunol.*, **19**, 378–387.

Wussling,M.H., Krannich,K., Landgraf,G., Herrmann-Frank,A., Wiedenmann,D., Gellerich,F.N. and Podhaisky,H. (1999) Sarcoplasmic reticulum vesicles embedded in agarose gel exhibit propagating calcium waves. *FEBS Lett.*, **463**, 103–109.

Zamzami,N., Brenner,C., Marzo,I., Susin,S.A. and Kroemer,G. (1998) Subcellular and submitochondrial mode of action of Bcl-2-like oncoproteins. *Oncogene*, **16**, 2265–2282.

Zhu,L., Ling,S., Yu,X.D., Venkatesh,L.K., Subramanian,T., Chinnadurai,G. and Kuo,T.H. (1999) Modulation of mitochondrial Ca^{2+} homeostasis by Bcl-2. *J. Biol. Chem.*, **274**, 33267–33273.

Received November 9, 2000; revised May 29, 2001; accepted June 13, 2001